THE JOURNAL OF PHYSICAL CHEMISTRY A

A: Kinetics, Dynamics, Photochemistry, and Excited States

Theoretical Investigations of Rate Coefficients of H + HO # OH + HO on a Full-Dimensional Potential Energy Surface

Xiaoxiao Lu, Xingan Wang, Bina Fu, and Donghui Zhang

J. Phys. Chem. A, **Just Accepted Manuscript** • DOI: 10.1021/acs.jpca.9b02526 • Publication Date (Web): 16 Apr 2019

ACS Publications

is published by the American Chemical Society. 1155 Sixteenth Street N.W., Washington, DC 20036

Theoretical Investigations of Rate Coefficients of H + H_2O_2 → OH + H_2O on a Full-Dimensional Potential Energy Surface

Xiaoxiao Lu,[†,‡] Xingan Wang,[‡] Bina Fu,[*,†] and Dong H. Zhang[*,†]

†*State Key Laboratory of Molecular Reaction Dynamics and Center for Theoretical and Computational Chemistry,Dalian Institute of Chemical Physics,Chinese Academy of Sciences,Zhongshan Road 457, Dalian 116023, China*

‡*Department of Chemical Physics, University of Science and Technology of China,Jinzhai Road 96, Hefei 230026, China*

E-mail: bina@dicp.ac.cn; zhangdh@dicp.ac.cn

Abstract

The thermal rate coefficients of $H + H_2O_2 \rightarrow OH + H_2O$ were obtained theoretically based on a recent fundamental invariant-neural network potential energy surface. The ring polymer molecular dynamics (RPMD) calculations were performed to get the rate coefficients with quantum effects, which are in good accord with some experimental values. The rate coefficients derived from extensive quasi-classical trajectory and canonical variational transition state calculations also predict well the experimental results at high temperatures. The RPMD rate coefficients for $H + H_2O_2 \rightarrow OH + H_2O$ are larger than $H + H_2O_2 \rightarrow H_2 + HO_2$, but at very low temperatures below the room temperature, the $H_2 + HO_2$ channel becomes dominant due to the significant quantum tunneling effects in the H atom transfer process. Considering that the old experimental values vary widely from different groups, we expect our theoretical investigations can motivate new experimental work which facilitates a more reliable comparison between theory and experiment.

Introduction

In order to get a deep insight into the combustion and explosion of hydrogen fuels, it is essential to have an accurate knowledge of the rates of various elementary reactions in combustion. In the past decades, the combustion system of H_2/O_2 was studied over a quite wide temperature range.[1–12] The $H + H_2O_2 \rightarrow OH + H_2O$ reaction plays a crucial role in combustion and atmospheric chemistry, since it produces hydroxyl radical which is the most reactive species of oxygen, and controls the atmospheric lifetime of most gases in the troposphere.[4]

An accurate determination of the rate coefficients of $H + H_2O_2 \rightarrow OH + H_2O$ is very important for the combustion model of H_2/O_2. The rate coefficients of the title reaction at various temperatures were recommended by several experimental research groups several decades ago.[1–8] For those experimental data, the rate coefficients at room temperature determined

by different laboratories[5–8] unexpectedly vary widely by almost one order of magnitude. Theoretically, the energies and stationary structures for the title reaction were determined based on low level of theory by Koussa *et al.*[9] Lamberts *et al.* calculated relative energies along the reaction path using various levels of theory, and employed the instanton theory to compute rate coefficients for the title reaction at very low temperatures down to 50K.[10] The canonical variational transition state theory with multidimensional tunneling[13–15] was used to compute the rate coefficients of this reaction.[11] In that work, the MPW1B95/MG3 level of theory that yields a barrier height and reaction energy of this reaction, gives rate coefficients achieving good agreement with the experiments by Baldwin *et al.*[1–3] However, the rate coefficients evaluated by the multireference perturbation theory (MRMP2) at the infinite basis set limit agree well with experimental results determined by Klemm *et al.*[6] These uncertainties involved in experimental and theoretical studies on the title reaction have motivated us to investigate this reaction further with more robust results.

From the theoretical point of view, full-dimensional quantum dynamics can predict the most accurate rate coefficients. For instance, high-dimensional quantum wave packet approaches were successfully applied to many small chemical reactive systems.[16–21] However, such first-principle calculations are limited to relatively small systems, owing to the tremendous computational efforts. Approximate methods have been developed[22–29] to incorporate important quantum effects, which are capable of producing accurate rate coefficients for larger systems over the past two decades. One of those is the ring-polymer molecular dynamics (RPMD) approch,[25–29] which employs the similarity between a quantum system and an artificial classical ring polymer. This ring polymer is composed of harmonically connected beads. Although the evolution of these beads obeys Newtonian dynamics, the RPMD simulations have proven to be accurate in describing the quantum effects, such as zero-point energy (ZPE) and quantum tunneling. The RPMD approach has been employed to calculate rate coefficients for many polyatomic reactions,[12,30–47] demonstrating that the RPMD method is able to give fairly accurate rate coefficients even at low temperatures.

In this work, the RPMD method was employed to calculate the rate coefficients of H + H_2O_2 → OH + H_2O. For comparison, we also performed quasi-classical trajectory (QCT) calculations as well as canonical variational transition state theory (CVT) calculations with small curvature tunneling (SCT) corrections. All the calculations were performed based on the accurate full-dimensional PES[48] by fundamental invariant-neural network (FI-NN) fitting to extensive UCCSD(T)-F12b/aug-cc-pVTZ energy points.[49] The recently reported rate coefficients of another product channel, namely, H + H_2O_2 → H_2 + HO_2, agree well with most of the experimental data, indicating the accuracy of our full-dimensional PES and kinetics simulations.[12]

This paper is organized as follows. Section gives an introduction of the FI-NN PES and computational approaches, together with numerical details of this work. Section gives the results of the present theoretical calculations, as well as the comparison of theoretical rate coefficients with experiment. Finally, the conclusions are given in Section .

Computational Details

Potential Energy Surface

The rate coefficients are investigated with the recently constructed full-dimensional PES.[48] The PES was constructed by FI-NN method based on roughly 114000 *ab initio* energy points, which were calculated at the UCCSD(T)-F12b/AVTZ level of theory.[49] For the H_3O_2 molecular system, there are 26 fundamental invariants with the maximum degree of 6. Thus, the PES was fitted using the 26 invariants as the input vector of the 26-50-60-1 NN structure, resulting in a small RMSE of 0.13 kcal/mol.[48] The PES of the H + H_2O_2 reaction covers both H_2 + HO_2 and OH + H_2O product channels. For comparison, the energies recommended by Lamberts *et al.*[10] and on the current PES are listed in Table 1. Small differences (around 1 kcal/mol of reaction energies were found. However, the activation energy of the title reaction varies widely. Nonetheless, our results agree well with those calculated by high

levels of theory such as UCCSD(T)-F12/cc-pVTZ-F12. It is interesting that the activation energy calculated by the UCCSD(T)-F12 theory is in good accord with the value obtained by the MPW1B95/MG3S method, but the reaction energy is over 1 kcal/mol higher for the MPW1B95/MG3S method.

The minimum energy path curves for the two reaction channels, $H + H_2O_2 \rightarrow OH + H_2O$ and $H + H_2O_2 \rightarrow H_2 + HO_2$, are shown in Fig. 1, which are compared with those results calculated based on the UCCSD(T)-F12b/AVTZ level of theory. We can see the FI-NN PES reproduces very well the *ab initio* data points, with a maximum fitting error of 0.1 kcal/mol. The collision of H and H_2O_2 either proceeds *via* a barrier (TS1) of 6.25 kcal/mol, resulting in $OH + H_2O$, or proceeds *via* a barrier (TS2) of 9.80 kcal/mol, leading to the $H_2 + HO_2$ products. The $H + H_2O_2$ reaction yields dominantly the $OH + H_2O$ product channel because of the lower reaction barrier and much larger reaction exothermicity ($\sim$71 kcal/mol). We recently reported the rate coefficients of $H + H_2O_2 \rightarrow H_2 + HO_2$,[12] by performing RPMD, QCT and CVT/SCT calculations. The results agree well with most of the experimental results, strongly supporting the accuracy of the FI-NN PES. Here, the three approaches are employed to calculate the rate coefficients of another product channel, namely, $H + H_2O_2 \rightarrow OH + H_2O$.

Computational approaches of rate coefficients

All RPMD rate coefficients were calculated using the RPMDrate code.[50] Here only some important equations are given since the RPMD theory has been described in detail elsewhere.[26–28,30,51–53] The Hamiltonian of the title reaction can be written as follows:

$$H(\mathbf{p},\mathbf{r}) = \sum_{i=1}^{5} \frac{\mathbf{p}_i^2}{2m_i} + V(\mathbf{r}_1,\mathbf{r}_2,...,\mathbf{r}_5) \quad (1)$$

where $\mathbf{p}_i$, $\mathbf{r}_i$ and m_i are the momentum, position and mass of atom i, and $V(\mathbf{r}_1,\mathbf{r}_2,...,\mathbf{r}_5)$ is the FI-NN PES of the title reactive system. Based on the isomorphism between the statistical

properties of the quantum system and those of a fictitious classical ring polymer,[25–28] the RPMD Hamiltonian can be written as follows:

$$H_n(\mathbf{p},\mathbf{r}) = \sum_{i=1}^{5}\sum_{j=1}^{n}\left(\frac{\left|\mathbf{p}_i^{(j)}\right|^2}{2m_i} + \frac{1}{2}m_i\omega_n^2\left|\mathbf{r}_i^{(j)} - \mathbf{r}_i^{(j-1)}\right|^2\right) + \sum_{j=1}^{n} V\left(\mathbf{r}_1^{(j)}, \mathbf{r}_2^{(j)}, ..., \mathbf{r}_5^{(j)}\right). \quad \mathbf{r}_i^{(0)} \equiv \mathbf{r}_i^{(n)} \tag{2}$$

Here, the superscript j represents the quantity of the jth bead, and $\omega_n = (\beta_n\hbar)^{-1}$ $\left(\beta_n = (nk_{\mathrm{B}}T)^{-1}\right)$ represents the force constant between two neighboring beads. The RPMD rate coefficient[27,28,30,50] can be expressed as the equation below, using the Bennett-Chandler factorization.[54,55]

$$k_{\mathrm{RPMD}}(T) = k_{\mathrm{QTST}}(T,\xi^{\ddagger}) \cdot \kappa(t\to\infty, T, \xi^{\ddagger}). \tag{3}$$

In Eq. (3), the first term $k_{\mathrm{QTST}}(T,\xi^{\ddagger})$ is the rate coefficient of centroid-density quantum transition state theory, representing the static contribution. This factor is calculated using the form of the centroid potential of mean force (PMF) :

$$k_{\mathrm{QTST}}(T,\xi^{\ddagger}) = 4\pi R_{\infty}^2\left(\frac{k_{\mathrm{B}}T}{2\pi\mu}\right)^{\frac{1}{2}} \cdot \exp\left(-\frac{\Delta W^{(n)}(T)}{k_{\mathrm{B}}T}\right) \tag{4}$$

Here, R_{∞} is a variable, which should be large enough to guarantee the interaction between the reactants is negligible, and $\Delta W^{(n)} = W^{(n)}(\xi^{\ddagger}) - W^{(n)}(0)$ represents the difference of free energy between the reactants and the dividing surface, which is usually computed by the umbrella integration[56–58] along ξ. The second term $\kappa\left(t\to\infty, T, \xi^{\ddagger}\right)$ is the transmission coefficient (recrossing factor), which accounts for the recrossing at the peak position $(\xi^{\ddagger})$ of the free-energy curve, representing a dynamical correction. Since the transmission coefficient always keeps constant after some evolution time, it can be approximated as $\kappa\left(t_p, T, \xi^{\ddagger}\right)$, where t_p is called the "plateau" time.

For comparison, we also performed the QCT and CVT/SCT computations to obtain the rate coefficients. The QCT thermal rate coefficient[59] can be expressed as the following

equation

$$k_{\mathrm{QCT}}(T) = \pi b_{\mathrm{max}}^2 \sqrt{\frac{8k_{\mathrm{B}}T}{\pi\mu}} \cdot \frac{N_{\mathrm{r}}}{N_{\mathrm{total}}}. \quad (5)$$

Here, the ratio of the numbers of reactive (N_{r}) and total trajectories (N_{total}) gives the reaction probability at a given temperature, and b_{max} represents the maximum impact parameter. In this trajectory-based calculations, we sampled the initial conditions of each trajectory from a Boltzmann distribution as implemented in VENUS,[59] including the translational energy and ro-vibrational states. In addition, the CVT/SCT rate coefficients were investigated using POLYRATE procedure.[15] The configurations of stationary points employed in the CVT/SCT calculations were obtained on the FI-NN PES.[48] As suggested by previous investigations,[11,60] the unharmonic torsion only affects slightly the rate coefficients at very high temperature, and thus the torsional vibrational modes of the H_2O_2 reactant and the transition state were treated with the harmonic oscillator model in this work. In fact, the torsional effects can result in a fortuitous cancellation of error, due to the simple harmonic oscillator for torsion vibrational modes of both the reactant and the transition state. This is different from the OH+CH_4 reaction,[61,62] where one additional hindered rotor exists at the transition state, but not at the reactants. More technical details can be found in literature.[14,15,63]

Numerical Details

For the calculations of free energy barriers, the reaction coordinate ($\xi \in$[-0.05,1.05]) is divided using a constant interval of 0.01 for the umbrella sampling, while using different force constants of the biasing potential of the transmission coefficient κ. For the title reaction, the free-energy curve is relatively flat in the reaction entrance channel but steep near the barrier. Therefore, $k_0 = 2.727(T \cdot \mathrm{K}^{-1})$ eV was used in the asymptotic region with ξ ranging from -0.05 to 0.78 at all temperatures and k_0 was also used at 200 and 300 K for each sampling window. Larger force constants were used near the energy barrier with steep slopes with ξ ranging from 0.79 to 1.05 in the temperature region of [500,1000]K. In detail, $2k_0$, $3k_0$ and

$4k_0$ were employed at 500 K, 700 K and 1000 K, respectively. The Andersen thermostat was chosen for simulating a constant temperature environment with a default sampling time of 100 fs. A total of 100 trajectories for each umbrella sampling window were launched by equilibrating in the Andersen thermostat for 10 ps, and then were propagated for 50 ps with a time interval of 0.1 fs.

After calculating the free-energy barrier, the optimal reaction coordinate ($\xi\dagger$) was determined at a given temperature. The transmission coefficient was computed at the barrier ($\xi\dagger$). Specifically, a long "parent" trajectory was performed in the presence of Andersen thermostat for 20 ps to obtain a series of constrained configurations, where the RATTLE algorithm[64] was employed. The time step is 0.1 fs. Each of these configurations constrained at the dividing surface with a sampling of 2 ps is served as the initial position of a "child" trajectory. After that, 100 "child" trajectories were propagated for 0.05 ps without the constraint and Andersen thermostat. The initial momentum of each child trajectory was randomly sampled from Maxwell distribution. Overall, a total of 100 000 child trajectories were spawned.

The QCT rate coefficients for this reaction were determined in the temperature region of [300,1000]K according to Eq. (5). The maximum impact parameter (b_{max}) was chosen by running a set of trajectories with trial values at a specified temperature. Usually, more trajectories were needed at low temperatures because of lower reaction probabilities. Furthermore, b_{max} at high temperatures are larger than those at low temperatures. For instance, the maximum impact parameter is 6.82 Bohr, 8.52 Bohr and 9.05 Bohr at 300, 500 and 700 K, respectively. The reaction probability at 1000 K is relatively large (0.08%) with a larger maximum impact parameter of 10.32 Bohr. The trajectories were initiated at a separation of $\sqrt{x^2+b^2}$ (x = 11.0 Bohr) between the centers of mass of two reactant fragments, and ended up with a centroid distance of two product fragments of 13 Bohr. The Velocity-Verlet integration algorithm was introduced into the QCT trajectory evolution. For each QCT trajectory, the maximum evolution time was set to 50 ps with a time interval of 0.073 fs. The total energy of every trajectory is conserved within 0.05 kcal/mol. We run extensive QCT

trajectories at low temperatures due to the extremely low reaction probabilities, leading to a small convergence error of less than 1%. At 300 K, only one reactive trajectory was found after running ∼250 000 trajectories. Roughly a total of 1.0×10^{10} and 1.0×10^{6} trajectories were computed at 300 K and 1000 K, respectively. The QCT rate coefficients were not calculated at temperatures lower than 300 K because of the huge computational cost.

Results and Discussions

Convergence Inspections of RPMD

In order to obtain accurate RPMD rate coefficients of the reaction, we first carefully checked the convergence of the free-energy barriers. Fig. 2(a) and Fig. 2(b) show the PMFs with respect to different numbers of ring-polymer beads at 200 and 700 K, respectively. The calculations performed with 1 bead provide the classical limit. Obviously, both of the two classical free-energy barrier heights are considerably higher than those obtained with larger number of beads, implying that quantum mechanical effects on the determination of the free-energy barrier are prominent. It can be reasonably assumed that quantum tunneling and ZPE effects have great influence on the current reaction. At 200 K, the free-energy barrier height of 0.23 eV with respect to 8 beads is much smaller than that obtained with 16 beads by ∼12 meV, while $\Delta W^{(n=16)}$ is also smaller than $\Delta W^{(n=32)}$ by ∼9 meV, indicating that more beads are necessary to converge the ΔW. From Figure 2(a), we can see that the free-energy barrier with 64 beads is well-converged because the curves acquired with 32 and 64 beads are almost coincident.

Furthermore, a series of RPMD simulations with different number of beads were also accomplished to obtain a well-converged free-energy barrier at 700 K. In Fig. 2(b), the free-energy barrier height gradually decreases with the increase of the number of beads and finally converges. Different trends are seen at 200 K, where the $\Delta W^{(n\geq 8)}$ as a function of number of beads is monotonically increasing. The ΔW calculated with 8 beads is 1.7 meV

smaller than that with 16 beads, which will only introduce 9% errors to exp(-$\beta\Delta W$). Hence, a total of 16 beads at 700 K are sufficiently large to make the free-energy barrier converged. By comparing the convergence behavior of the free-energy barriers at 200 and 700 K, we presumed that more beads are needed for the reaction at low temperatures than at high temperatures. We thus verified that $n = 16$ is sufficiently large for 1000 K after careful convergence inspections.

The well-converged free-energy curves in the temperature region ($T \in$ [200,1000]K) are plotted in Figure 3, where two apparent trends can be found. First, the reaction coordinates of all free energy barriers are around 1.0, implying that the title reaction is thermally activated near the barrier. Second, the free-energy barrier height is a monotonically increasing function of the reaction temperature, which increases from 0.25 eV to 0.79 eV in the temperature region of [200, 1000]K.

After the convergence inspections for free-energy, we employed the same useful strategy to obtain well-converged transmission coefficients values. As shown in Fig. 4(a) for the results at 200 K, one can find that the $\kappa^{(n)}(t, \xi^{\ddagger})$ with different ring polymer beads decrease rapidly with time and keeps constant over 20 fs, similar to the behaviour of $\kappa^{(n)}(t, \xi^{\ddagger})$ at 700 K in Fig. 4(b). The classical transmission coefficient obtained with one bead at 200 K is very close to 1.0. Nevertheless, the RPMD recrossing factors (n = 8, 16, 32, 64) are all smaller than 0.11. Such significant differences reveal that the quantum-statistical effects in the title reaction can strongly influence the recrossing factor at low temperatures. In contrast, at 700 K, the classical transmission coefficient is only ~1.03 times $\kappa^{(n>=16)}$, suggesting that the quantum effects on the recrossing factor at high temperatures are not so important as at low temperatures.

At 200 K, the transmission coefficient becomes well-converged with 64 beads since $\kappa^{(n=64)}$ is roughly 3% larger than $\kappa^{(n=32)}$. By comparing the $\kappa^{(n)}$ obtained by different number of beads, we can see that the number of beads has great effect on $\kappa^{(n)}$ at the low temperature. However, $\kappa^{(n)}$ converges more quickly at higher reaction temperature. For example, $\kappa^{(n=8)}$ is

nearly converged, seen from its comparison with $\kappa^{(n=16)}$ at 700 K. After convergence check, 32 and 16 beads were employed to calculate the RPMD transmission coefficients at 300 K and in the temperature region of [500,1000]K, respectively.

Figure 5 shows the converged time-dependence transmission coefficients in the temperature region of [200,1000]K. At medium and high temperatures ($T \in [500, 1000]$K), the transmission coefficients changes mildly with a maximum difference of roughly 0.03. For instance, the transmission coefficient is 0.905 at 1000 K and 0.896 at 700 K. Apparently, the $\kappa(t)$ monotonically increases from 0.109 at 200 K to 0.905 at 1000 K as the temperature rises. In an overall view, the growth rate is slowing down gradually. In addition, there are remarkable differences between the transmission coefficient at $T = 200$ K and the other results at $T \geq 300$ K, implying the quantum effects have great influences on the reactivity at temperatures below the calculated crossover temperature ($T_c = 315$ K) in this work.

Rate Coefficients

In Figure 6(a), the RPMD rate coefficients for the title reaction are compared with other theoretical results obtained using the QCT and CVT/SCT approaches in an Arrhenius plot, together with the previous experimental results. We can find that the RPMD results agree well with the CVT/SCT values at temperatures below 400 K, indicating the CVT/SCT approach describes quite well the tunneling effect at low temperatures for this reaction. The QCT result at 300 K achieves excellent agreement with the corresponding RPMD result. These three theoretical rate coefficients at 300 K are in good coincidence with the experimental result by Gorse and Volman. However, the experimentally measured values at around room temperature from Meagher *et al.*, Michael *et al.* and Klemm group are dramatically larger than those computed by RPMD, QCT and CVT/SVT methods. Since the reaction probability is tiny for temperatures below 300 K, we did not obtain the QCT rate coefficients at low temperatures. However, seen from the slope and trend of the QCT curve, the QCT rate coefficients below 300 K should be smaller than the corresponding RPMD results,

which results from the absent tunneling effects in QCT calculations. Interestingly, the QCT and RPMD rate coefficient curves intersect around 300 K, which agree quite well with the crossover temperature of roughly 315 K of the title reaction as we mentioned above. Our calculations for another product channel $H+H_2O_2 \rightarrow H_2+HO_2$ also show a intersection between the QCT and RPMD curves,[12] which predicts well the crossover temperature of about 544 K.

When the temperature increases further, we can see two trends of theoretical rate coefficients. First, the Arrhenius plot of RPMD shows an excellent coincidence with the experimental value determined by Forst *et al.* at $T = 700$ K and by Gorse and Volman at $T = 300$ K. The QCT and CVT/SVT results are larger than RPMD results at 400 K $\leq T \leq$ 1000 K, particularly, the QCT rate coefficient at $T = 1000$ K are larger than the RPMD value by nearly one order of magnitude. The overestimation of rate from QCT is probably due to the ZPE leakage of reactants and transition state, as well as the ZPE violation of products in QCT calculations. Note that the soft-ZPE treatment of products was employed in counting the reactive trajectories.[12,48] Additionally, those experimental rate coefficients measured by Baldwin *et al.* agree well with the results of QCT and CVT/SCT, with a deviation of around 12%.

We also plotted the rate coefficients of the title reaction at very low temperatures down to 50 K in Fig. 6(b), which were calculated by Lamberts *et al* using the instanton theory.[10] We can find good agreement between the present RPMD rate coefficients and the corresponding instanton rate coefficients at the temperature region of ([200,250]K), for which the deviations are less than 40%. Based on the trend and slope of the RPMD and instanton rate coefficient curves, the two batches of theoretical results obtained from different theories show good accordance.

To compare the reactivity of $H+H_2O_2 \rightarrow OH+H_2O$ and $H+H_2O_2 \rightarrow H_2+HO_2$ at various temperatures, we depicted the RMPD rate coefficients of two product channels in Fig. 7. At temperatures higher than 300 K, the rate coefficients of the $OH+H_2O$ channel is larger than

those of H_2+HO_2 by a factor of around 1 to 3, due to the lower reaction barrier and much larger reaction exothermicity of the OH+H_2O channel. However, at low temperatures below the room temperature, the situation inverses, as the rate coefficients of H_2+HO_2 becomes larger. Particulary at T = 200 K, the rate coefficient of H_2+HO_2 is larger than that of OH+H_2O by a factor of roughly 4. This is not surprising because at very low temperatures the quantum tunneling effects dominate the reactivity. The H+H_2O_2→H_2+HO_2 reaction is a H atom transfer process, which involves more significant tunneling effects than an OH transfer process in H+H_2O_2→ OH+H_2O. This is consistent with the higher crossover temperature of H_2+HO_2 than that of OH+H_2O as well.

Conclusions

In summary, we reported the rate coefficients of the H + H_2O_2 → OH + H_2O reaction on the FI-NN PES[48] using three theoretical approaches, including RPMD, QCT and CVT/SCT. For the RPMD calculations, we set different number of beads to compute the free energy barrier and transmission coefficients in the temperature region of [200,1000]K after careful convergence inspections. Because the available experimental data varies widely, the present RPMD results show good agreement with some experimental data. The RPMD rate coefficients reproduce well the experimental values recommended by Forst *et al.* and Gorse *et al.* at T = 300 K, and that by Forst *et al.* at T = 700 K. The QCT rate coefficient around 300 K agrees excellent well with the RPMD result. However, the QCT rate coefficients below 300 K are presumed to be smaller than the corresponding RPMD results, which results from the neglect of tunneling effects in QCT calculations. Due to the ZPE issues embedded in the QCT approach, the QCT results are larger than RPMD results above 300 K. In addition, the calculated QCT and CVT/SCT rates around 700 K are all in reasonably good accord with experimental values measured by Baldwin in 1967 and 1970. Furthermore, we found the rate coefficients of H + H_2O_2 → OH + H_2O are larger than those of H+H_2O_2→H_2+HO_2 above

300 K, due to the lower barrier and larger reaction exothermicity of the OH + H_2O channel, but below the room temperature, the H_2+HO_2 channel dominates due to more substantial quantum tunneling effects in the H atom transfer process. Overall, the available experimental data varies widely for the both product channels of the H+H_2O_2 reaction. New experiment is expected to provide a more reliable comparison between theory and experiment.

Acknowledgement

We thank Qingyong Meng for many useful discussions on the RPMD calculations. This work was supported by the National Key R&D Program of China (Grant No. 2016YFF0200500), the National Natural Science Foundation of China (Grant Nos. 21722307, 21673233, 21433009, 21688102), the Strategic Priority Research Program of the Chinese Academy of Sciences (Grant no. XDB17000000).

References

(1) Baldwin, R. R.; Brattan, D.; Tunnicliffe, B.; Walker, R. W.; Webster, S. J. The hydrogen-sensitized decomposition of hydrogen peroxide. *Combust. Flame* **1970**, *15*, 133–142.

(2) Baldwin, R. R.; Walker, R. W. Rate constants for hydrogen + oxygen system, and for H atoms and OH radicals + alkanes. *J. Chem. Soc. Faraday Trans. 1 Phys. Chem. Condens. Phases* **1979**, *75*, 140–154.

(3) Baldwin, R. R.; Jackson, D.; Walker, R. W.; Webster, S. J. Interpretation of the slow reaction and second limit of hydrogen oxygen mixtures by computer methods. *Trans. Faraday Soc.* **1967**, *63*, 1676–1686.

(4) Forst, W.; Giguere, P. A. Inhibition by Hydrogen Peroxide of the Second Explosion Limit of the Hydrogen-Oxygen Reaction. *J. Phys. Chem.* **1958**, *62*, 340–343.

(5) Gorse, R. A.; Volman, D. H. Photochemistry of the gaseous hydrogen peroxideâĂŤcarbon monoxide system. II: Rate constants for hydroxyl radical reactions with hydrocarbons and for hydrogen atom reactions with hydrogen peroxide. *J. Photochem.* **1974**, *3*, 115–122.

(6) Klemm, R. B.; Payne, W. A.; Stief, L. J. Absolute rate parameters for the reaction of atomic hydrogen with H_2O_2. 1st Symp. Chem. Kinet. Data Up. Low. Atmos. New York, 1975; pp 61–72.

(7) Meagher, J. F.; Heicklen, J. The photolysis of hydrogen peroxide in the presence of carbon monoxide. *J. Photochem.* **1974**, *3*, 455–466.

(8) Michael, J. V.; Whytock, D. A.; Lee, J. H.; Payne, W. A.; Stief, L. J. Absolute rate constant for the reaction of atomic chlorine with hydrogen peroxide vapor over the temperature range 265-400 K. *J. Chem. Phys.* **1977**, *67*, 3533–3536.

(9) Koussa, H.; Bahri, M.; Jaïdane, N.; Ben Lakhdar, Z. Kinetic study of the reaction H_2O_2+H $\rightarrow$$H_2O$+OH by ab initio and density functional theory calculations. *J. Mol. Struct. Theochem* **2006**, *770*, 149–156.

(10) Lamberts, T.; Samanta, P. K.; Kohn, A.; Kastner, J. Quantum tunneling during interstellar surface-catalyzed formation of water: the reaction H + H_2O_2 $\rightarrow$ H_2O + OH. *Phys. Chem. Chem. Phys.* **2016**, *18*, 33021–33030.

(11) Ellingson, B. A.; Theis, D. P.; Tishchenko, O.; Zheng, J.; Truhlar, D. G. Reactions of Hydrogen Atom with Hydrogen Peroxide. *J. Phys. Chem. A* **2007**, *111*, 13554–13566.

(12) Lu, X.; Meng, Q.; Wang, X.; Fu, B.; Zhang, D. H. Rate coefficients of the H + H_2O_2 $\rightarrow$ H_2 + HO_2 reaction on an accurate fundamental invariant-neural network potential energy surface. *J. Chem. Phys.* **2018**, *149*, 174303.

(13) Truhlar, D. G.; Garrett, B. C. Variational transition-state theory. *Acc. Chem. Res.* **1980**, *13*, 440–448.

(14) Melissas, V. S.; Truhlar, D. G. Deuterium and carbon-13 kinetic isotope effects for the reaction of OH with CH_4. *J. Chem. Phys.* **1993**, *99*, 3542–3552.

(15) Lu, D.-h.; Truong, T. N.; Melissas, V. S.; Lynch, G. C.; Liu, Y.-P.; Garrett, B. C.; Steckler, R.; Isaacson, A. D.; Rai, S. N.; Hancock, G. C. et al. POLYRATE 4: A new version of a computer program for the calculation of chemical reaction rates for polyatomics. *Comput. Phys. Commun.* **1992**, *71*, 235–262.

(16) Fu, B.; Zhang, D. H. Mode specificity in the H + H_2O → H_2 + OH reaction: A full-dimensional quantum dynamics study. *J. Chem. Phys.* **2013**, *138*, 184308.

(17) Zhou, Y.; Zhang, D. H. Eight-dimensional quantum reaction rate calculations for the H+CH_4 and H_2+CH_3 reactions on recent potential energy surfaces. *J. Chem. Phys.* **2014**, *141*, 194307.

(18) Fu, B.; Zhang, D. H. A full-dimensional quantum dynamics study of the mode specificity in the H + HOD abstraction reaction. *J. Chem. Phys.* **2015**, *142*, 64314.

(19) Sun, P.; Zhang, Z.; Chen, J.; Liu, S.; Zhang, D. H. Well converged quantum rate constants for the H_2 + OH → H_2O + H reaction via transition state wave packet. *J. Chem. Phys.* **2018**, *149*, 64303.

(20) González-Lezana, T.; Larrégaray, P.; Bonnet, L.; Wu, Y.; Bian, W. The dynamics of the C(^{1}D)+H_2/D_2/HD reactions at low temperature. *J. Chem. Phys.* **2018**, *148*, 234305.

(21) Ellerbrock, R.; Manthe, U. Full-dimensional quantum dynamics calculations for H + CHD_3 → H_2 + CD_3: The effect of multiple vibrational excitations. *J. Chem. Phys.* **2018**, *148*, 224303.

(22) Bao, J. L.; Truhlar, D. G. Variational transition state theory: theoretical framework and recent developments. *Chem. Soc. Rev.* **2017**, *46*, 7548–7596.

(23) Liu, J.; Miller, W. H. A simple model for the treatment of imaginary frequencies in chemical reaction rates and molecular liquids. *J. Chem. Phys.* **2009**, *131*, 74113.

(24) Hele, T. J. H.; Althorpe, S. C. Derivation of a true (t $\rightarrow$ 0+) quantum transition-state theory. I. Uniqueness and equivalence to ring-polymer molecular dynamics transition-state-theory. *J. Chem. Phys.* **2013**, *138*, 084108.

(25) Chandler, D.; Wolynes, P. G. Exploiting the isomorphism between quantum theory and classical statistical mechanics of polyatomic fluids. *J. Chem. Phys.* **1981**, *74*, 4078–4095.

(26) Craig, I. R.; Manolopoulos, D. E. Quantum statistics and classical mechanics: Real time correlation functions from ring polymer molecular dynamics. *J. Chem. Phys.* **2004**, *121*, 3368–3373.

(27) Craig, I. R.; Manolopoulos, D. E. Chemical reaction rates from ring polymer molecular dynamics. *J. Chem. Phys.* **2005**, *122*, 84106.

(28) Craig, I. R.; Manolopoulos, D. E. A refined ring polymer molecular dynamics theory of chemical reaction rates. *J. Chem. Phys.* **2005**, *123*, 34102.

(29) Habershon, S.; Manolopoulos, D. E.; Markland, T. E.; III, T. F. M. Ring-Polymer Molecular Dynamics: Quantum Effects in Chemical Dynamics from Classical Trajectories in an Extended Phase Space. *Annu. Rev. Phys. Chem.* **2013**, *64*, 387–413.

(30) Collepardo-Guevara, R.; Suleimanov, Y. V.; Manolopoulos, D. E. Bimolecular reaction rates from ring polymer molecular dynamics. *J. Chem. Phys.* **2009**, *130*, 174713.

(31) Suleimanov, Y. V.; Collepardo-Guevara, R.; Manolopoulos, D. E. Bimolecular reaction rates from ring polymer molecular dynamics: Application to H + CH_4 $\rightarrow$ H_2 + CH_3. *J. Chem. Phys.* **2011**, *134*, 44131.

(32) de Tudela, R.; Aoiz, F. J.; Suleimanov, Y. V.; Manolopoulos, D. E. Chemical Reaction Rates from Ring Polymer Molecular Dynamics: Zero Point Energy Conservation in Mu + H_2 → MuH + H. *J. Phys. Chem. Lett.* **2012**, *3*, 493–497.

(33) Allen, J. W.; Green, W. H.; Li, Y.; Guo, H.; Suleimanov, Y. V. Communication: Full dimensional quantum rate coefficients and kinetic isotope effects from ring polymer molecular dynamics for a seven-atom reaction OH + CH_4 → CH_3 + H_2O. *J. Chem. Phys.* **2013**, *138*, 221103.

(34) Li, Y.; Suleimanov, Y. V.; Li, J.; Green, W. H.; Guo, H. Rate coefficients and kinetic isotope effects of the X + CH_4 → CH_3 + HX (X = H, D, Mu) reactions from ring polymer molecular dynamics. *J. Chem. Phys.* **2013**, *138*, 94307.

(35) Li, Y.; Suleimanov, Y. V.; Green, W. H.; Guo, H. Quantum Rate Coefficients and Kinetic Isotope Effect for the Reaction Cl + CH_4 → HCl + CH_3 from Ring Polymer Molecular Dynamics. *J. Phys. Chem. A* **2014**, *118*, 1989–1996.

(36) de Tudela, R.; Suleimanov, Y. V.; Richardson, J. O.; Sáez Rábanos, V.; Green, W. H.; Aoiz, F. J. Stress Test for Quantum Dynamics Approximations: Deep Tunneling in the Muonium Exchange Reaction D + HMu → DMu + H. *J. Phys. Chem. Lett.* **2014**, *5*, 4219–4224.

(37) Suleimanov, Y. V.; Kong, W. J.; Guo, H.; Green, W. H. Ring-polymer molecular dynamics: Rate coefficient calculations for energetically symmetric (near thermoneutral) insertion reactions (X + H_2) → HX + H(X = C(^{1}D), S(^{1}D)). *J. Chem. Phys.* **2014**, *141*, 244103.

(38) Hickson, K. M.; Loison, J.-C.; Guo, H.; Suleimanov, Y. V. Ring-Polymer Molecular Dynamics for the Prediction of Low-Temperature Rates: An Investigation of the C(^{1}D) + H_2 Reaction. *J. Phys. Chem. Lett.* **2015**, *6*, 4194–4199.

(39) Meng, Q.; Chen, J.; Zhang, D. H. Communication: Rate coefficients of the H + CH_4 → H_2 + CH_3 reaction from ring polymer molecular dynamics on a highly accurate potential energy surface. *J. Chem. Phys.* **2015**, *143*, 101102.

(40) Arseneau, D. J.; Fleming, D. G.; Li, Y.; Li, J.; Suleimanov, Y. V.; Guo, H. Rate Coefficient for the $^4He\mu$ + CH_4 Reaction at 500 K: Comparison between Theory and Experiment. *J. Phys. Chem. B* **2016**, *120*, 1641–1648.

(41) Meng, Q.; Chen, J.; Zhang, D. H. Ring polymer molecular dynamics fast computation of rate coefficients on accurate potential energy surfaces in local configuration space: Application to the abstraction of hydrogen from methane. *J. Chem. Phys.* **2016**, *144*, 154312.

(42) Meng, Q.; Hickson, K. M.; Shao, K.; Loison, J.-C.; Zhang, D. H. Theoretical and experimental investigations of rate coefficients of $O(^1D)$ + CH_4 at low temperature. *Phys. Chem. Chem. Phys.* **2016**, *18*, 29286–29292.

(43) Suleimanov, Y. V.; Aoiz, F. J.; Guo, H. Chemical Reaction Rate Coefficients from Ring Polymer Molecular Dynamics: Theory and Practical Applications. *J. Phys. Chem. A* **2016**, *120*, 8488–8502.

(44) Zuo, J.; Li, Y.; Guo, H.; Xie, D. Rate Coefficients of the HCl + OH → Cl + H_2O Reaction from Ring Polymer Molecular Dynamics. *J. Phys. Chem. A* **2016**, *120*, 3433–3440.

(45) Hickson, K. M.; Suleimanov, Y. V. An experimental and theoretical investigation of the $C(^1D)$ + D_2 reaction. *Phys. Chem. Chem. Phys.* **2017**, *19*, 480–486.

(46) Thompson, K. M.; Gao, Y.; Marshall, P.; Wang, H.; Zhou, L.; Li, Y.; Guo, H. Experimental and theoretical studies of the reactions of ground-state sulfur atoms with hydrogen and deuterium. *J. Chem. Phys.* **2017**, *147*, 134302.

(47) Zuo, J.; Xie, C.; Guo, H.; Xie, D. Accurate Determination of Tunneling-Affected Rate Coefficients: Theory Assessing Experiment. *J. Phys. Chem. Lett.* **2017**, *8*, 3392–3397.

(48) Lu, X.; Shao, K.; Fu, B.; Wang, X.; Zhang, D. H. An accurate full-dimensional potential energy surface and quasiclassical trajectory dynamics of the H + H_2O_2 two-channel reaction. *Phys. Chem. Chem. Phys.* **2018**, *20*, 23095–23105.

(49) Knizia, G.; Adler, T. B.; Werner, H.-J. Simplified CCSD(T)-F12 methods: Theory and benchmarks. *J. Chem. Phys.* **2009**, *130*, 54104.

(50) Suleimanov, Y. V.; Allen, J. W.; Green, W. H. RPMDrate: Bimolecular chemical reaction rates from ring polymer molecular dynamics. *Comput. Phys. Commun.* **2013**, *184*, 833–840.

(51) Braams, B. J.; Manolopoulos, D. E. On the short-time limit of ring polymer molecular dynamics. *J. Chem. Phys.* **2006**, *125*, 124105.

(52) Hele, T. J. H.; Althorpe, S. C. Derivation of a true (t $\rightarrow$ 0+) quantum transition-state theory. I. Uniqueness and equivalence to ring-polymer molecular dynamics transition-state-theory. *J. Chem. Phys.* **2013**, *138*, 84108.

(53) Hele, T. J. H.; Suleimanov, Y. V. Should thermostatted ring polymer molecular dynamics be used to calculate thermal reaction rates? *J. Chem. Phys.* **2015**, *143*, 74107.

(54) Bennett, C. H. *Algorithms Chem. Comput.*; ACS Symposium Series; AMERICAN CHEMICAL SOCIETY, 1977; Vol. 46; pp 63–97.

(55) Chandler, D. Statistical mechanics of isomerization dynamics in liquids and the transition state approximation. *J. Chem. Phys.* **1978**, *68*, 2959–2970.

(56) Kästner, J.; Thiel, W. Bridging the gap between thermodynamic integration and umbrella sampling provides a novel analysis method: âĂIJUmbrella integrationâĂİ. *J. Chem. Phys.* **2005**, *123*, 144104.

(57) Kästner, J.; Thiel, W. Analysis of the statistical error in umbrella sampling simulations by umbrella integration. *J. Chem. Phys.* **2006**, *124*, 234106.

(58) Kästner, J. Umbrella integration in two or more reaction coordinates. *J. Chem. Phys.* **2009**, *131*, 34109.

(59) Hu, X.; Hase, W. L.; Pirraglia, T. Vectorization of the general Monte Carlo classical trajectory program VENUS. *J. Comput. Chem.* **1991**, *12*, 1014–1024.

(60) Ellingson, B. A.; Lynch, V. A.; Mielke, S. L.; Truhlar, D. G. Statistical thermodynamics of bond torsional modes: Tests of separable, almost-separable, and improved PitzerÍCGwinn approximations. *J. Chem. Phys.* **2006**, *125*, 084305.

(61) Li, J.; Guo, H. Thermal Rate Coefficients and Kinetic Isotope Effects for the Reaction OH + CH_4 → H_2O + CH_3 on an ab Initio-Based Potential Energy Surface. *J. Phys. Chem. A* **2018**, *122*, 2645–2652.

(62) Ellingson, B. A.; Pu, J.; Lin, H.; Zhao, Y.; Truhlar, D. G. Multicoefficient Gaussian-3 Calculation of the Rate Constant for the OH + CH_4 Reaction and Its $^{12}C/^{13}C$ Kinetic Isotope Effect with Emphasis on the Effects of Coordinate System and Torsional Treatment. *J. Phys. Chem. A* **2007**, *111*, 11706–11717.

(63) Battin-Leclerc, F.; Kim, I. K.; Talukdar, R. K.; Portmann, R. W.; Ravishankara, A. R.; Steckler, R.; Brown, D. Rate Coefficients for the Reactions of OH and OD with HCl and DCl between 200 and 400 K. *J. Phys. Chem. A* **1999**, *103*, 3237–3244.

(64) Andersen, H. C. Rattle: A âĂIJvelocityâĂ?version of the shake algorithm for molecular dynamics calculations. *J. Comput. Phys.* **1983**, *52*, 24–34.

(65) Baulch, D. L.; Bowman, C. T.; Cobos, C. J.; Cox, R. A.; Just, T.; Kerr, J. A.; Pilling, M. J.; Stocker, D.; Troe, J.; Tsang, W. et al. Evaluated Kinetic Data for Combustion Modeling: Supplement II. *J. Phys. Chem. Ref. Data* **2005**, *34*, 757–1397.

Table 1: Activation energies and reaction energies of the title reaction calculated by our group and Lamberts *et al* depending on various methods.[10] All values are given in kcal mol^{-1} excluding zero-point energies.

method	activation energy	reaction energy
UCCSD(T)-F12/cc-pVTZ-F12	6.09	-71.53
UCCSD(T)/cc-pVTZ	6.62	-70.34
icMRCCSD(T)/cc-pVTZ	5.95	-69.84
HEAT-456QP		-71.15
BHLYP/def2-TZVPD	6.50	-79.20
B3LYP/def2-TZVPD	2.58	-71.53
B3LYP/MG3S	2.67	-71.75
PBE0/def2-TZVPD	4.94	-68.83
PBE0/MG3S	5.11	-69.07
PWB6K/MG3S	8.60	-73.49
MPW1B95/MG3S	6.33	-69.74
M05-2X/MG3S	10.97	-72.49
UCCSD(T)-F12b/cc-pVTZ[a]	6.25	-71.09

[a] This work.

Figure Captions

Figure 1 The minimum energy paths for H + H_2O_2 → OH + H_2O and H + H_2O_2 → H_2 + HO_2 calculated from the FI-NN PES (solid lines) and those obtained from UCCSD(T)-F12b/AVTZ level of theory (symbols). The reaction coordinate is the signed distance along the reaction path from the saddle points.

Figure 2 (a) The free-energy curves with respect to different numbers of beads for H + H_2O_2 → OH + H_2O at 200 K. (b) The free-energy curves with respect to different numbers of beads for H + H_2O_2 → OH + H_2O at 700 K.

Figure 3 The free-energy curves as a function of reaction temperature for H + H_2O_2 → OH + H_2O.

Figure 4 (a) The transmission coefficients with respect to different numbers of beads for H + H_2O_2 → OH + H_2O at 200 K. (b) The transmission coefficients with respect to different numbers of beads for H + H_2O_2 → OH + H_2O at 700 K.

Figure 5 The transmission coefficients as a function of time for H + H_2O_2 → OH + H_2O.

Figure 6 (a) Comparison of rate coefficients (in $cm^3molecule^{-1}s^{-1}$) for the H + H_2O_2 → OH + H_2O reaction obtained from the RPMD , QCT and CVT/SCT approaches, together with the experimental rate coefficients recommended by Ref.[65] (b) the same as (a) except the results of instanton theory by Lamberts *et al*[10] at very low temperatures were included.

Figure 7 Comparison of RPMD rate coefficients (in $cm^3molecule^{-1}s^{-1}$) for H + H_2O_2 → OH + H_2O and H + H_2O_2 → H_2 + HO_2.[12]

Figure 1

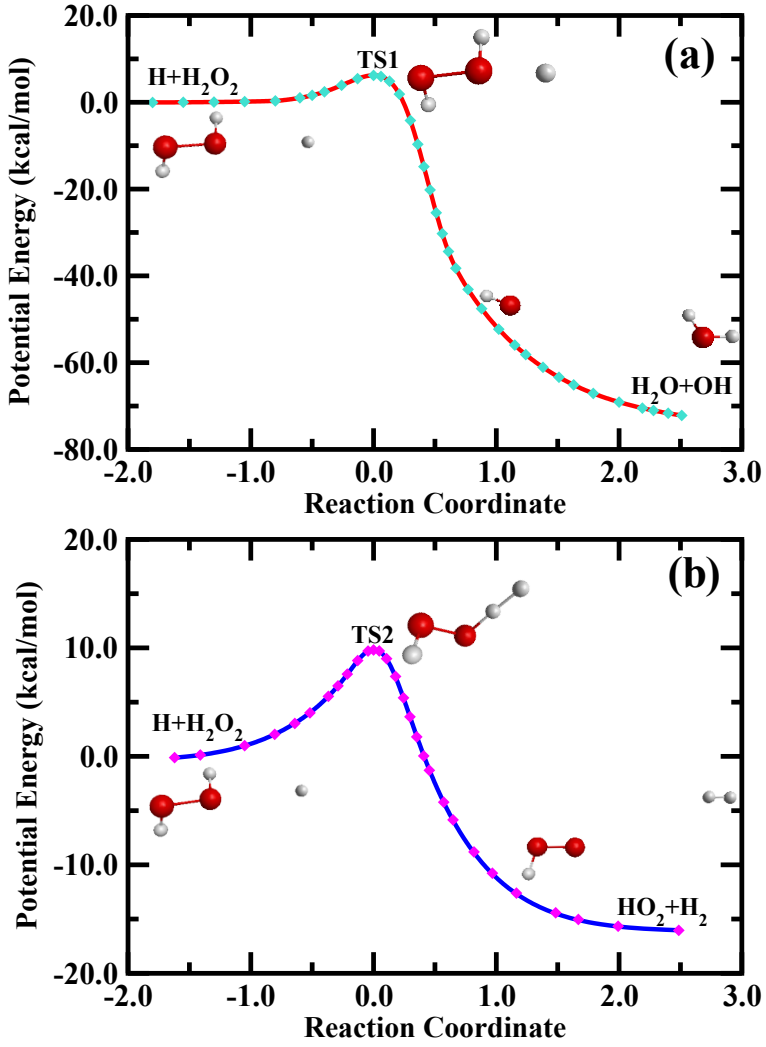
(a)
TS1
H+H2O2
H2O+OH
Potential Energy (kcal/mol)
Reaction Coordinate
20.0
0.0
-20.0
-40.0
-60.0
-80.0
-2.0
-1.0
0.0
1.0
2.0
3.0
(b)
TS2
H+H2O2
HO2+H2
Potential Energy (kcal/mol)
Reaction Coordinate
20.0
10.0
0.0
-10.0
-20.0

Figure 2

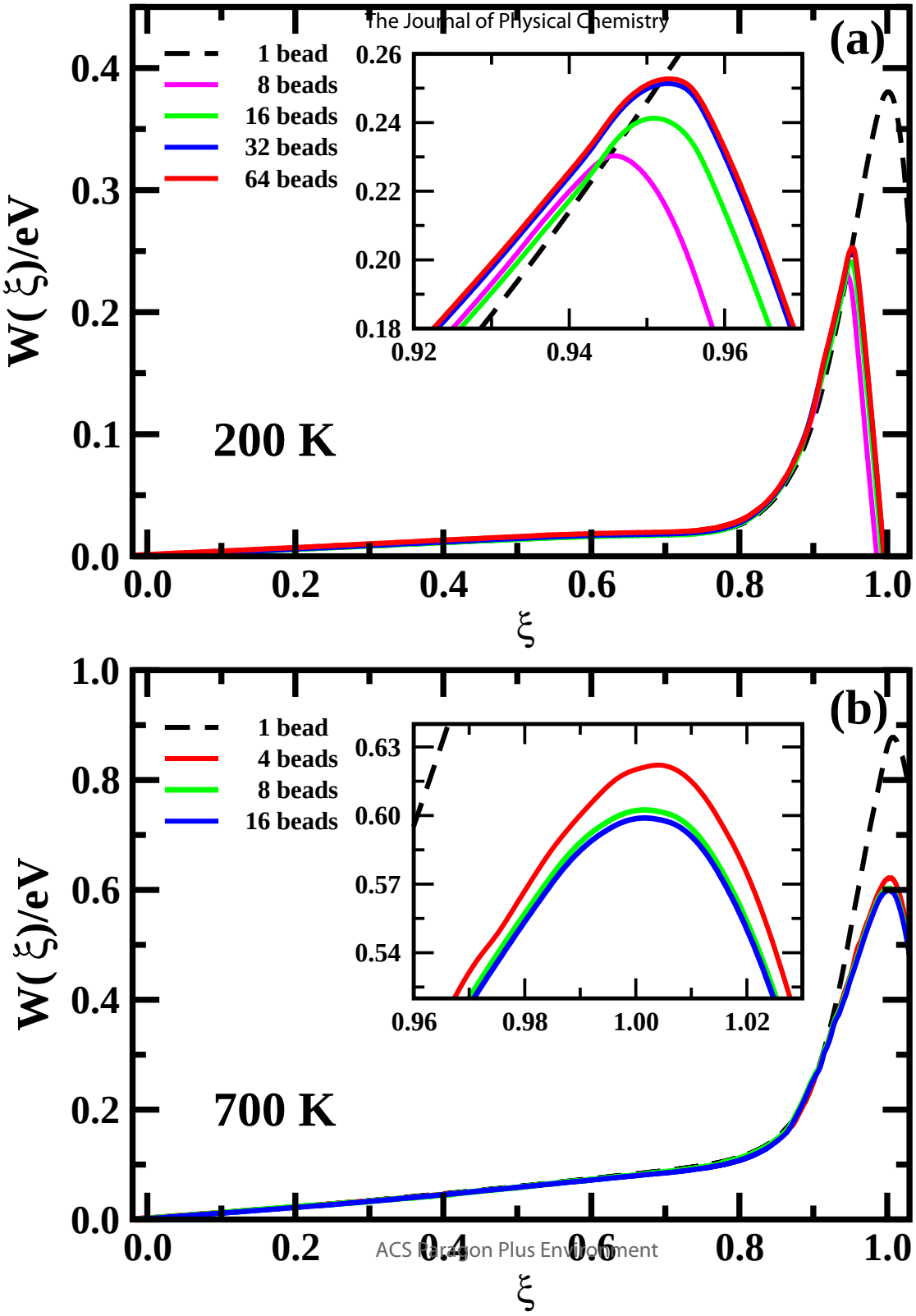
(a)
1 bead
8 beads
16 beads
32 beads
64 beads
200 K
W(ξ)/eV
ξ
(b)
1 bead
4 beads
8 beads
16 beads
700 K
W(ξ)/eV
ξ

Figure 3

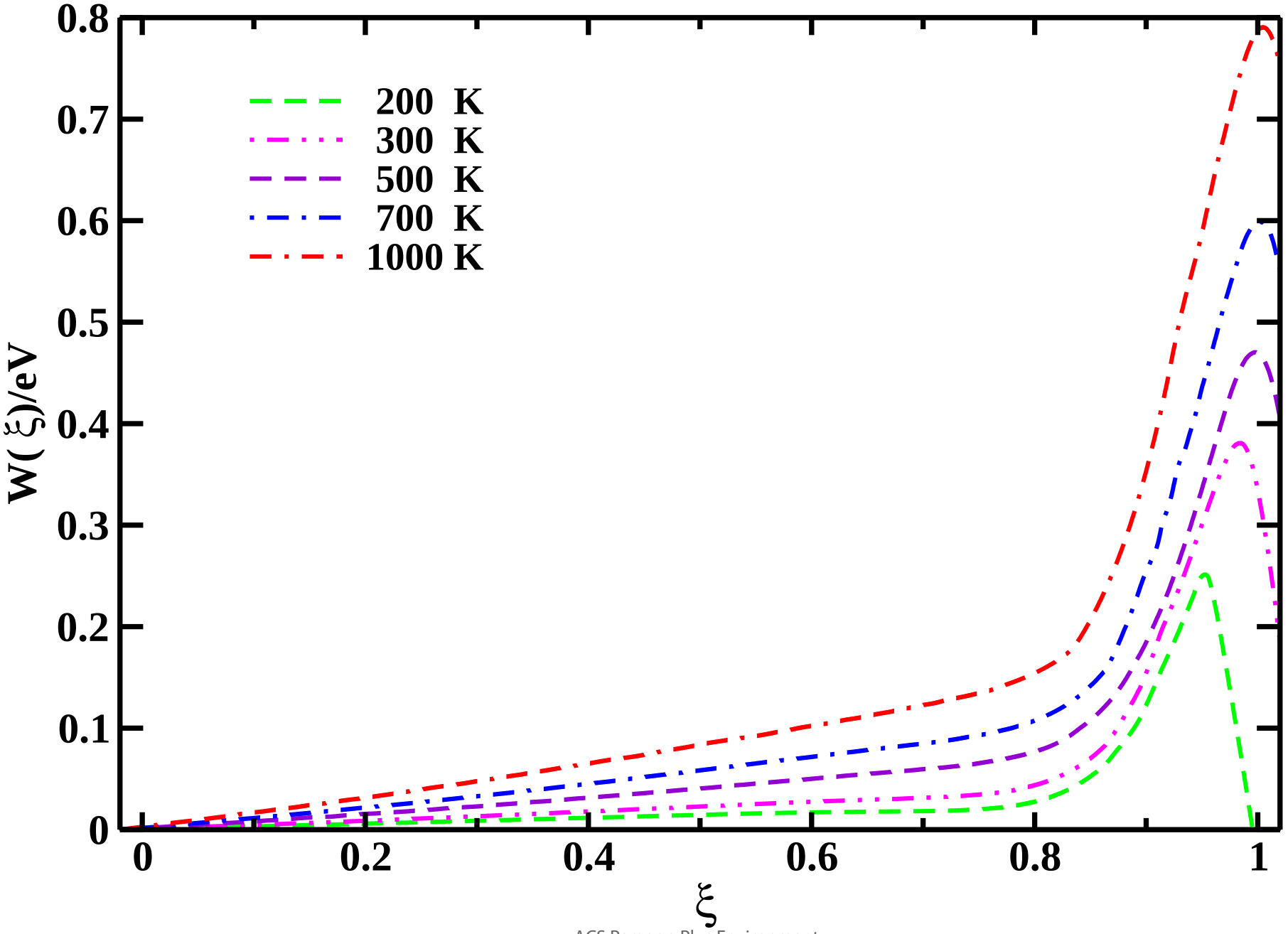
0.8
0.7
0.6
0.5
0.4
0.3
0.2
0.1
0
W(ξ)/eV
200 K
300 K
500 K
700 K
1000 K
0
0.2
0.4
0.6
0.8
1
ξ

Figure 4

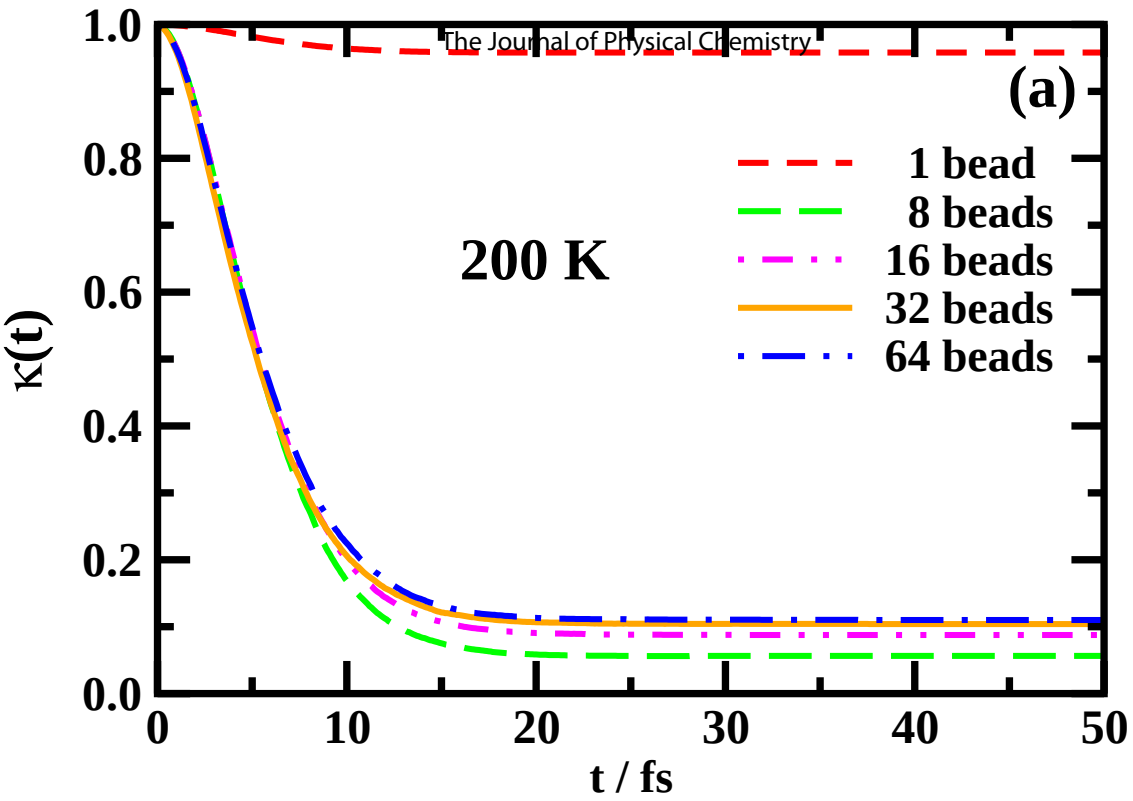
(a)
200 K
1 bead
8 beads
16 beads
32 beads
64 beads
κ(t)
t / fs
1.0
0.8
0.6
0.4
0.2
0.0
0
10
20
30
40
50

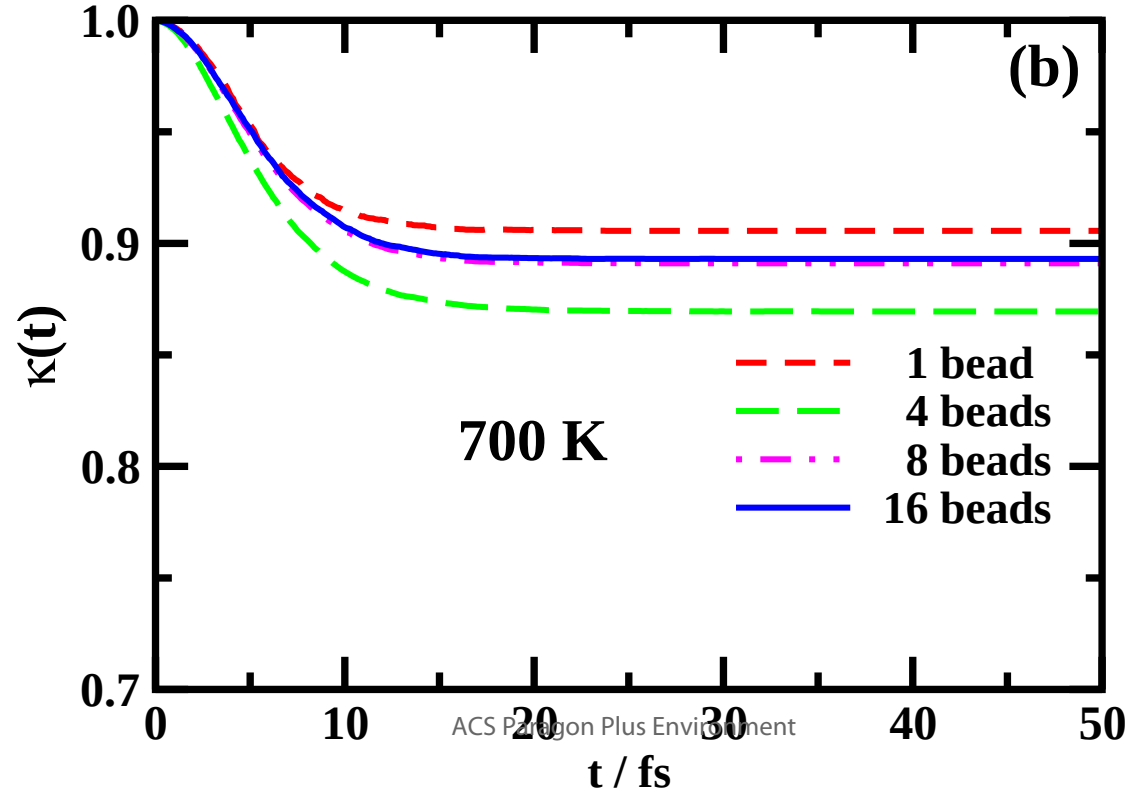
(b)
700 K
1 bead
4 beads
8 beads
16 beads
κ(t)
t / fs
1.0
0.9
0.8
0.7
0
10
20
30
40
50

Figure 5

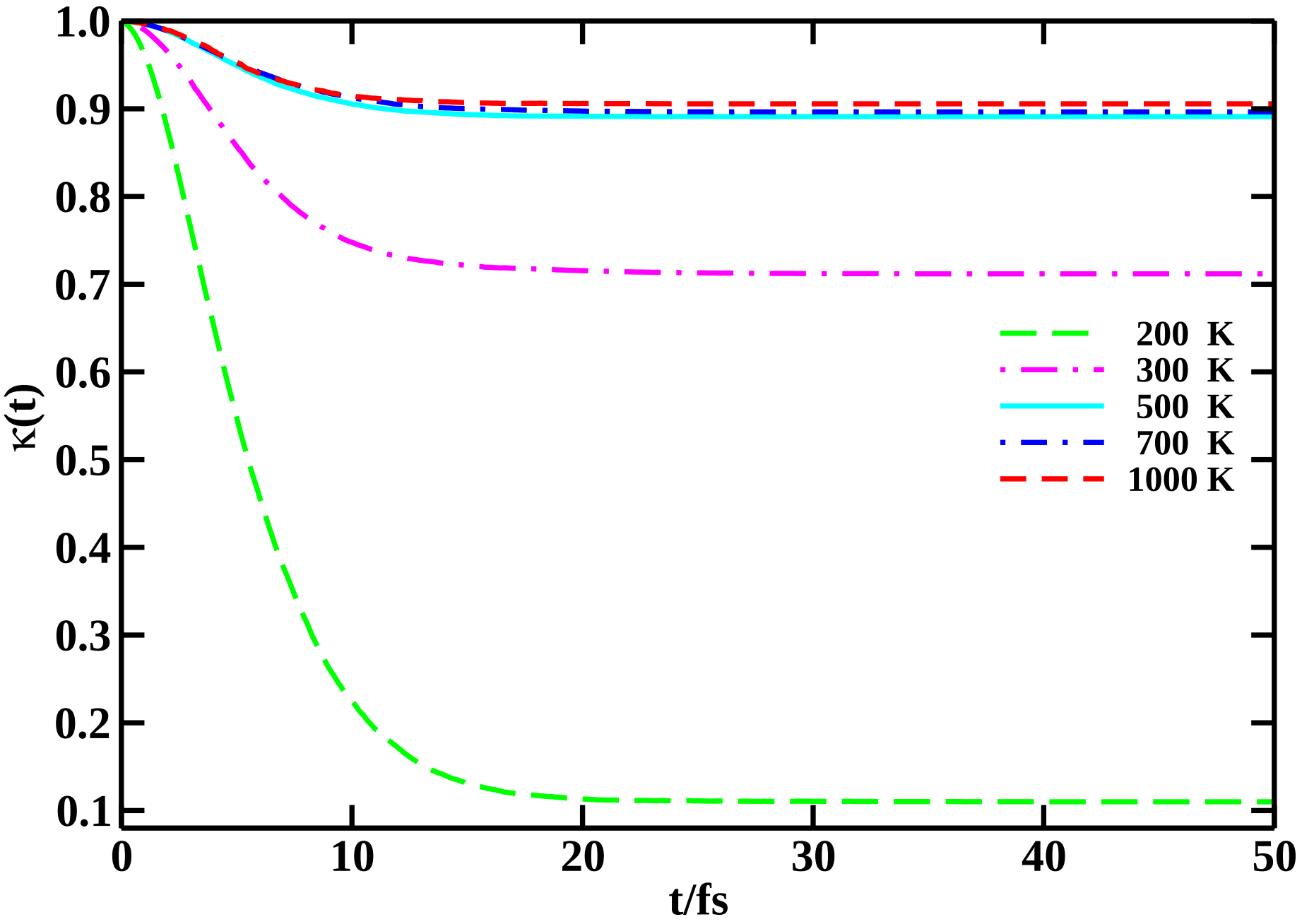
1.0
0.9
0.8
0.7
0.6
0.5
0.4
0.3
0.2
0.1
κ(t)
0
10
20
30
40
50
t/fs
200 K
300 K
500 K
700 K
1000 K

Figure 6

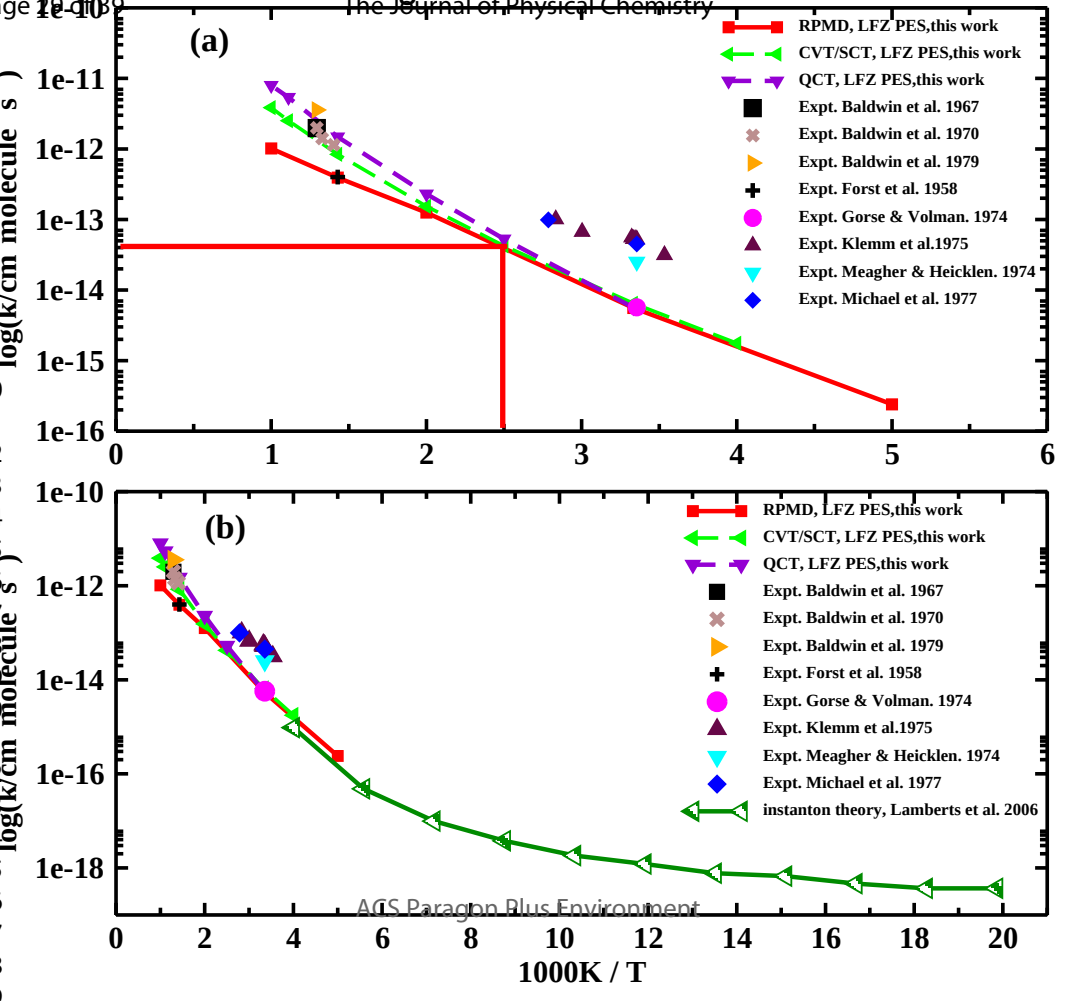

Figure 7

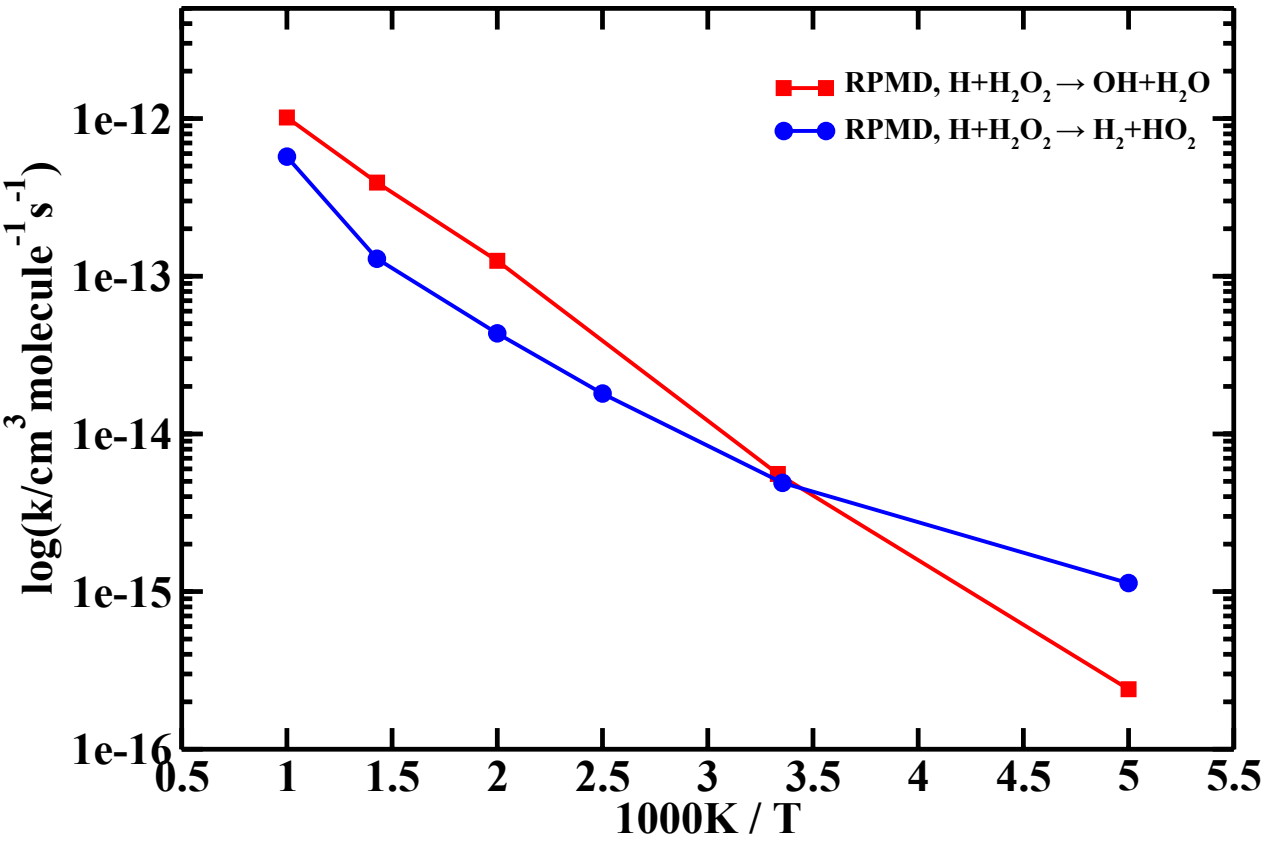
RPMD, H+H2O2 → OH+H2O
RPMD, H+H2O2 → H2+HO2
log(k/cm3molecule-1s-1)
1e-12
1e-13
1e-14
1e-15
1e-16
0.5
1
1.5
2
2.5
3
3.5
4
4.5
5
5.5
1000K / T

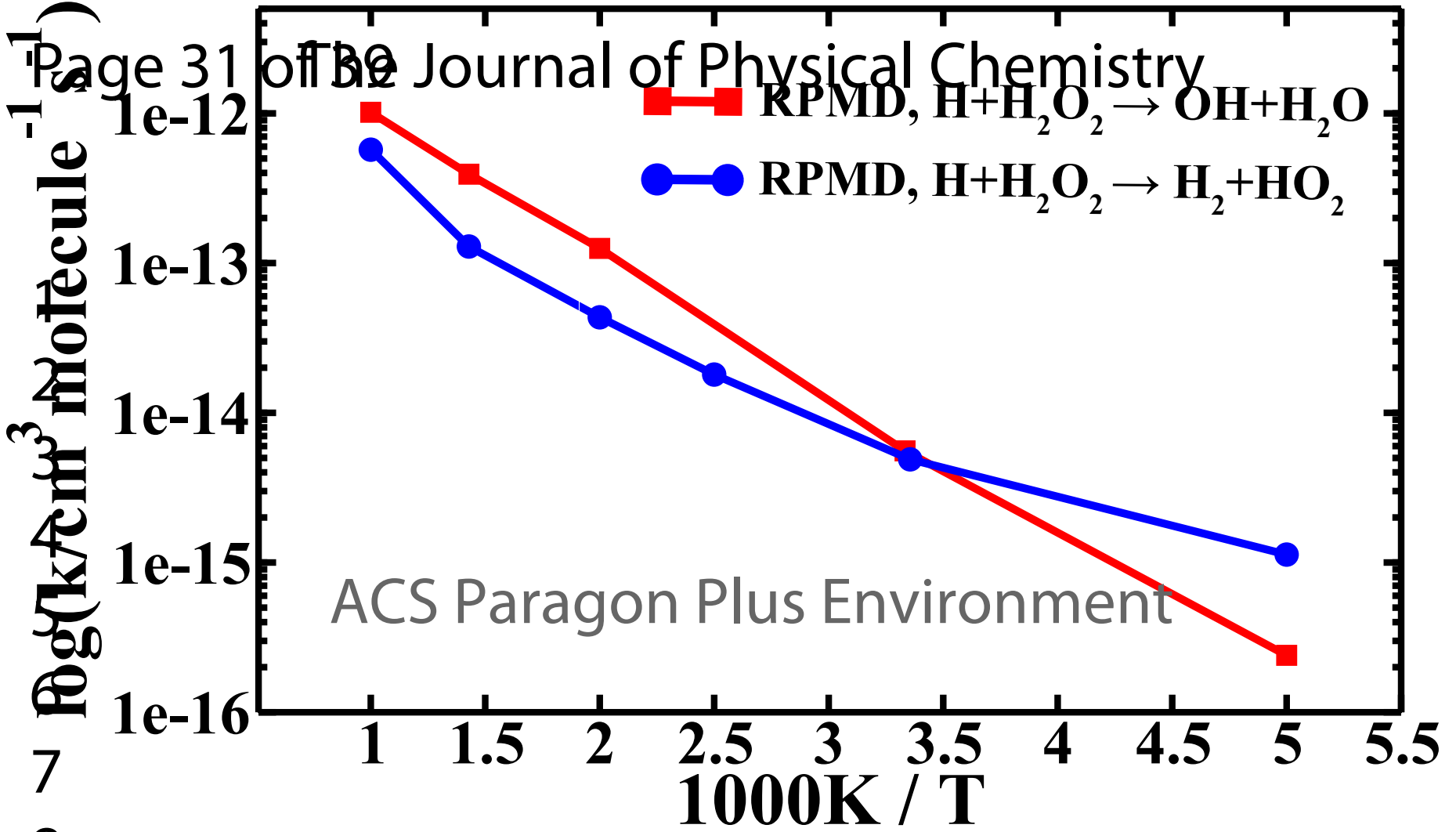
RPMD, H+H2O2 → OH+H2O
RPMD, H+H2O2 → H2+HO2
ACS Paragon Plus Environment
1e-12
1e-13
1e-14
1e-15
1e-16
1
1.5
2
2.5
3
3.5
4
4.5
5
5.5
1000K / T

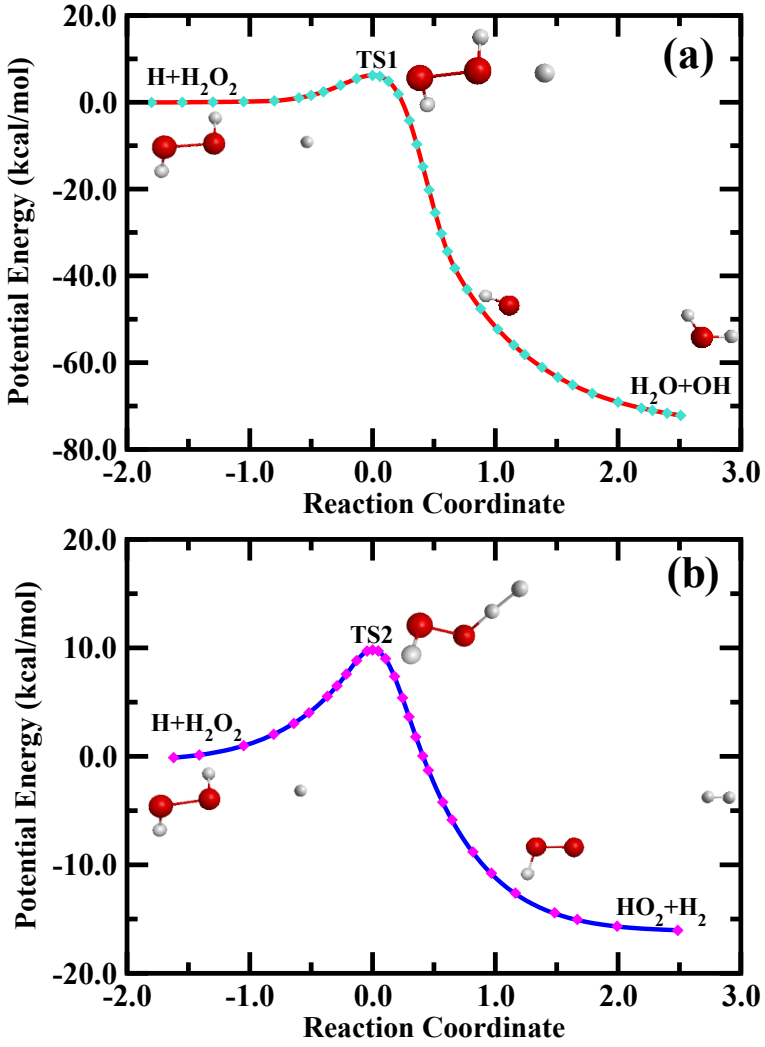
(a)
TS1
H+H2O2
H2O+OH
Potential Energy (kcal/mol)
Reaction Coordinate
20.0
0.0
-20.0
-40.0
-60.0
-80.0
-2.0
-1.0
0.0
1.0
2.0
3.0
(b)
TS2
H+H2O2
HO2+H2
Potential Energy (kcal/mol)
Reaction Coordinate
20.0
10.0
0.0
-10.0
-20.0

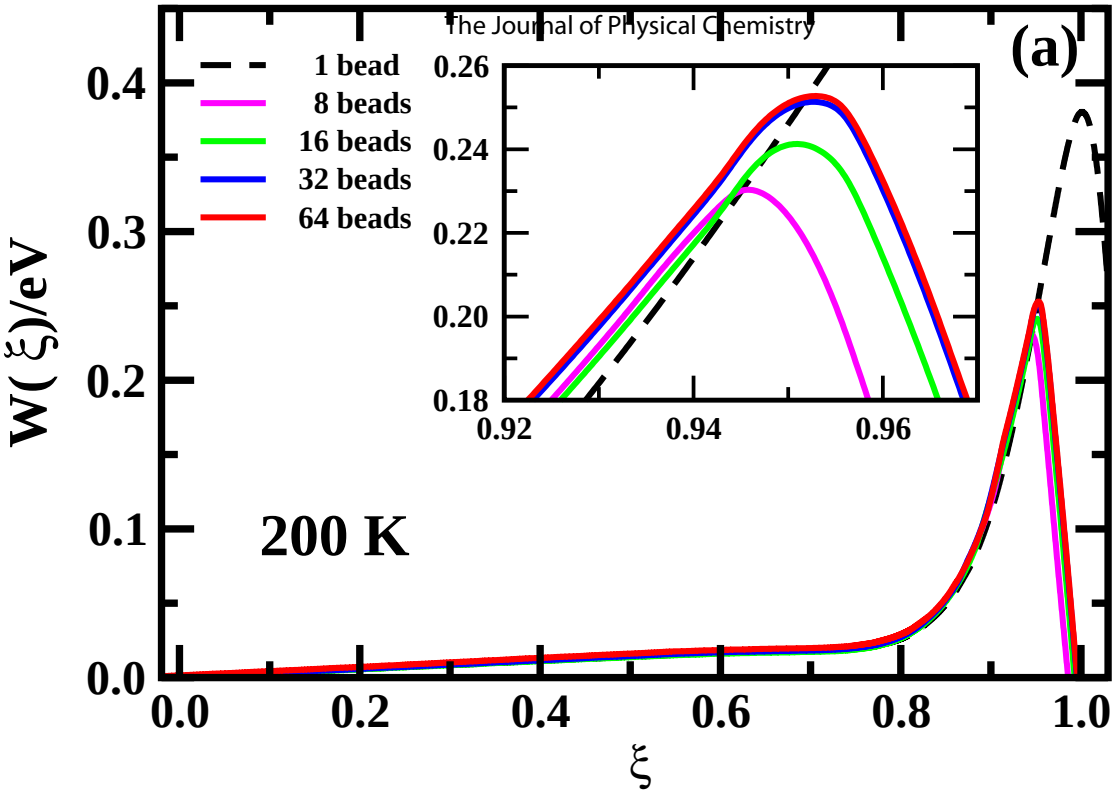
(a)
1 bead
8 beads
16 beads
32 beads
64 beads
200 K
W(ξ)/eV
ξ
0.0
0.1
0.2
0.3
0.4
0.6
0.8
1.0
0.18
0.20
0.22
0.24
0.26
0.92
0.94
0.96

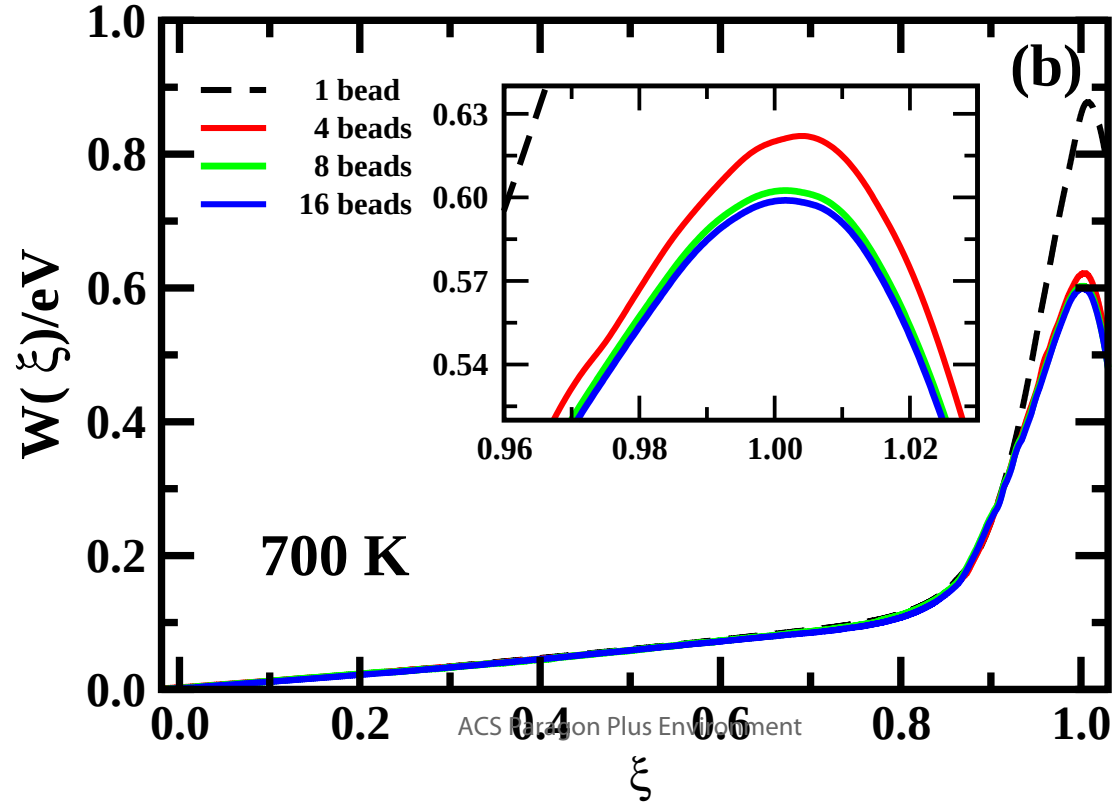
(b)
1 bead
4 beads
8 beads
16 beads
700 K
W(ξ)/eV
ξ
0.0
0.2
0.4
0.6
0.8
1.0
0.54
0.57
0.60
0.63
0.96
0.98
1.00
1.02

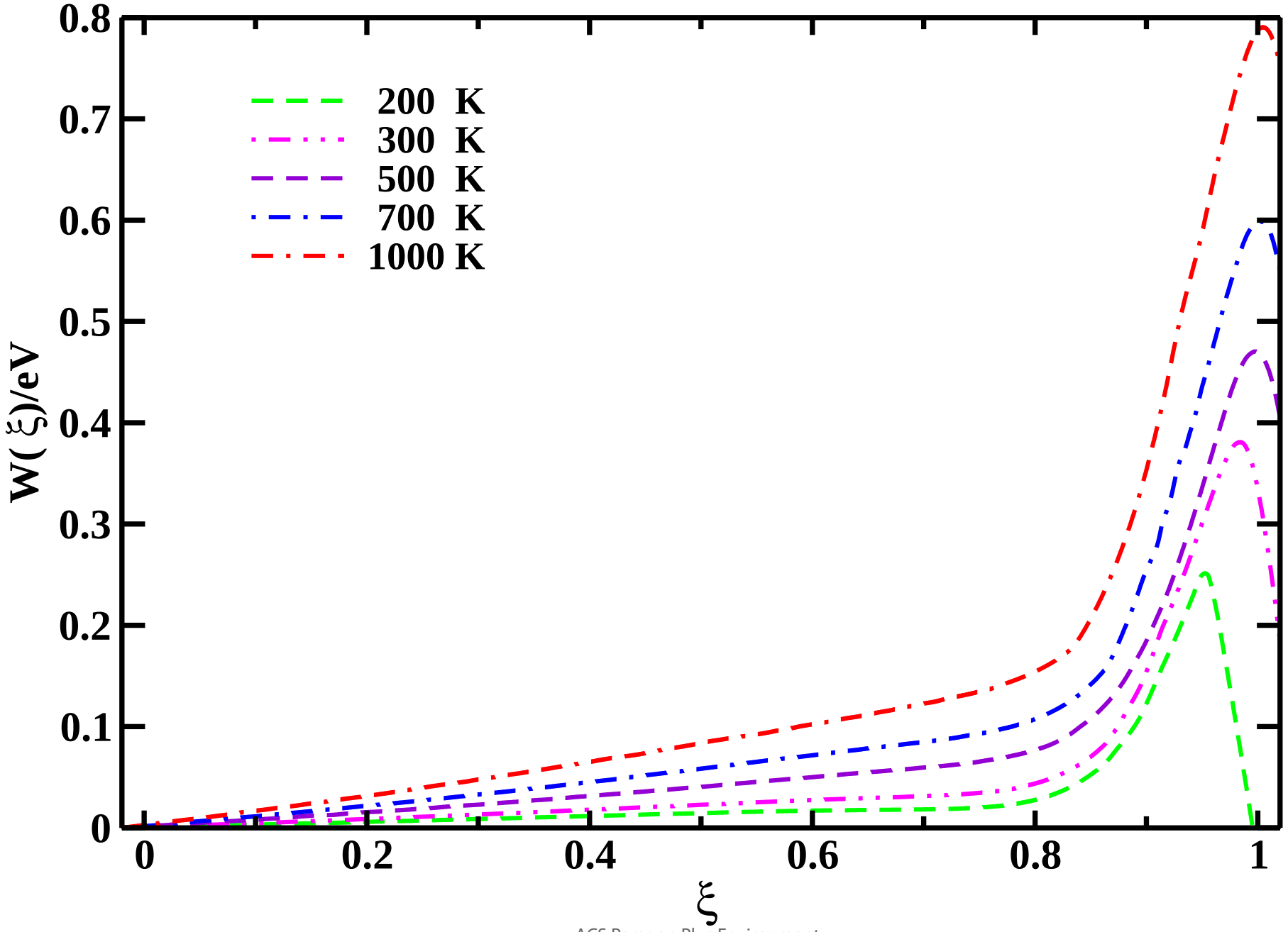
0.8
0.7
0.6
0.5
0.4
0.3
0.2
0.1
0
W(ξ)/eV
200 K
300 K
500 K
700 K
1000 K
0
0.2
0.4
0.6
0.8
1
ξ

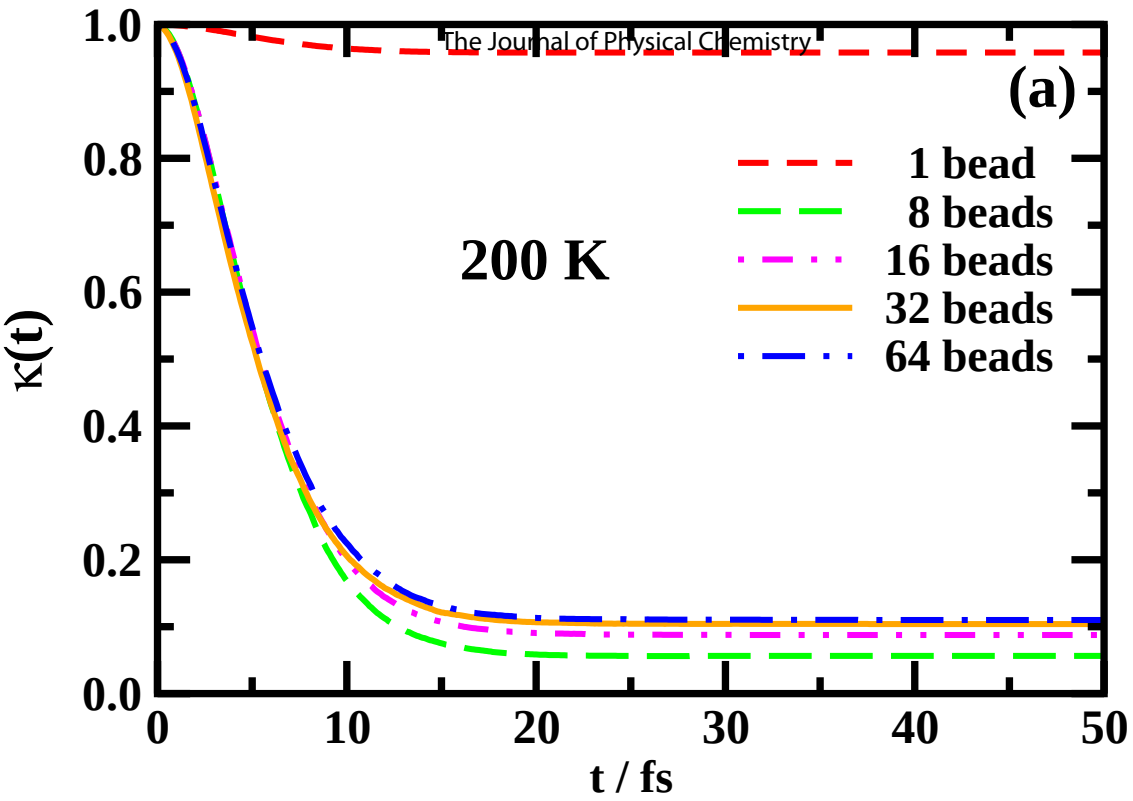
(a)
200 K
1 bead
8 beads
16 beads
32 beads
64 beads
κ(t)
t / fs
1.0
0.8
0.6
0.4
0.2
0.0
0
10
20
30
40
50

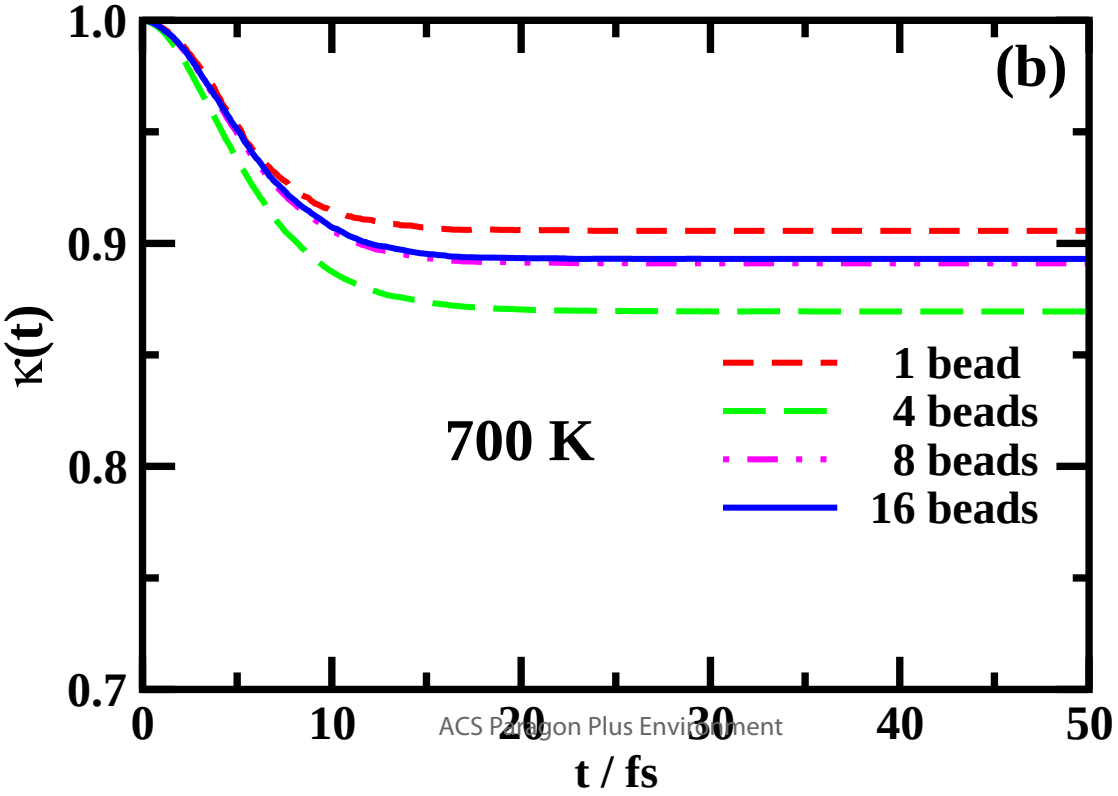
(b)
700 K
1 bead
4 beads
8 beads
16 beads
κ(t)
t / fs
1.0
0.9
0.8
0.7
0
10
20
30
40
50

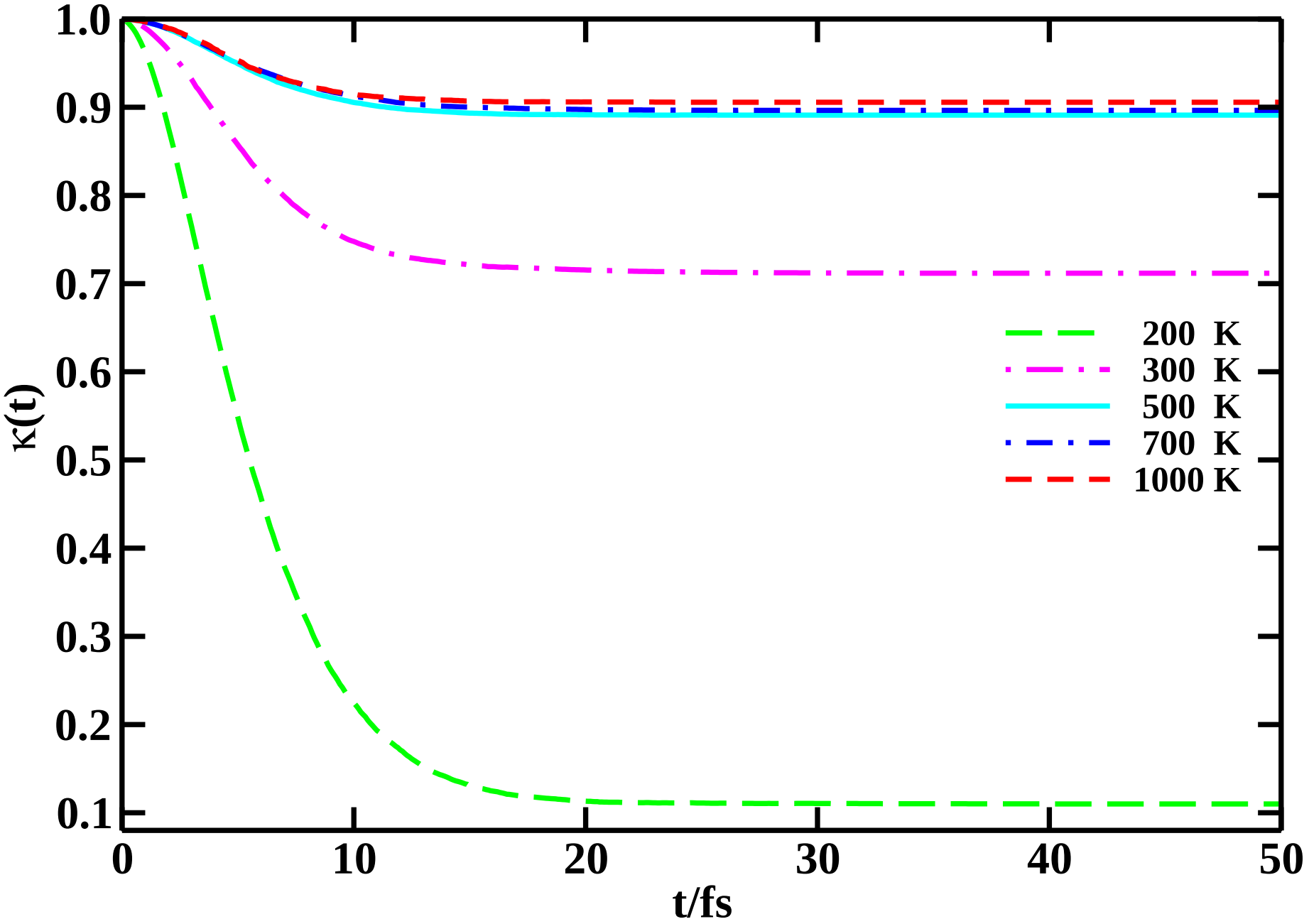
1.0
0.9
0.8
0.7
0.6
0.5
0.4
0.3
0.2
0.1
κ(t)
0
10
20
30
40
50
t/fs
200 K
300 K
500 K
700 K
1000 K

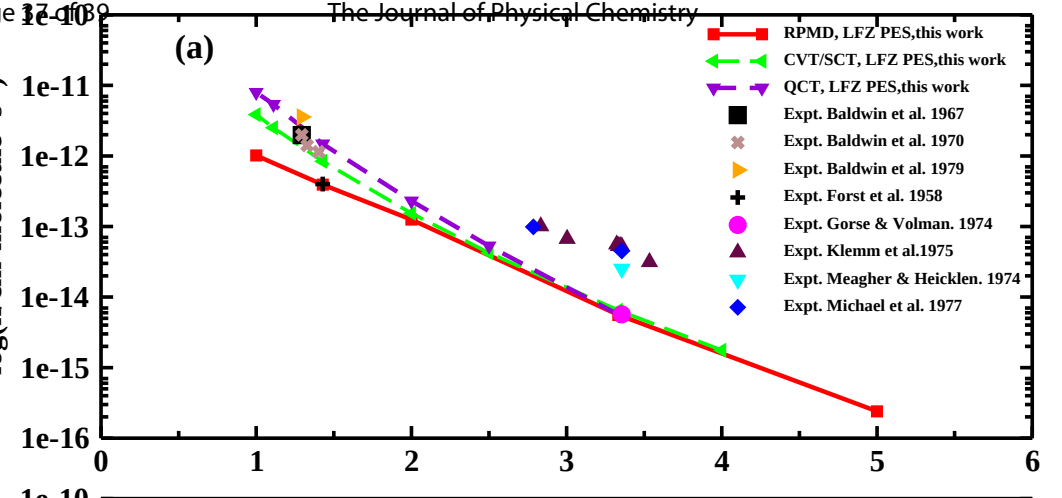

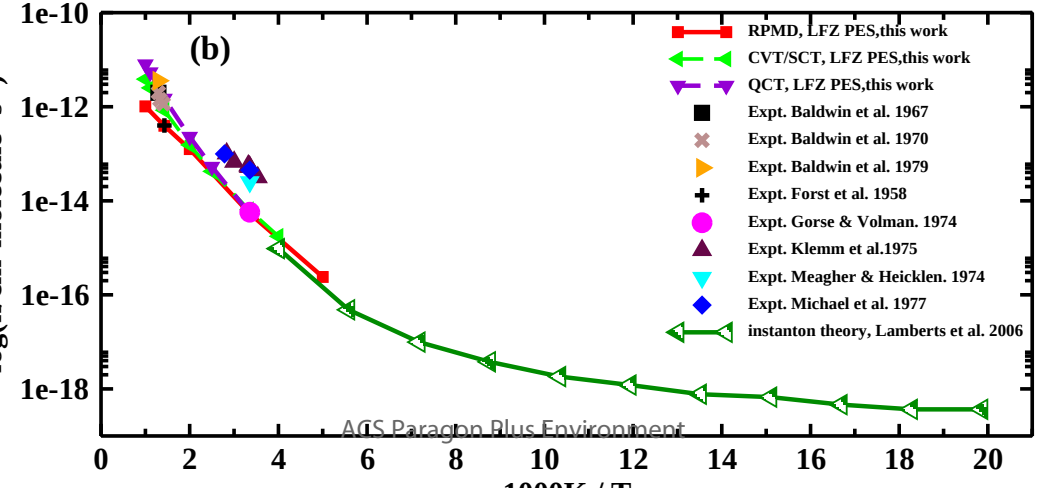

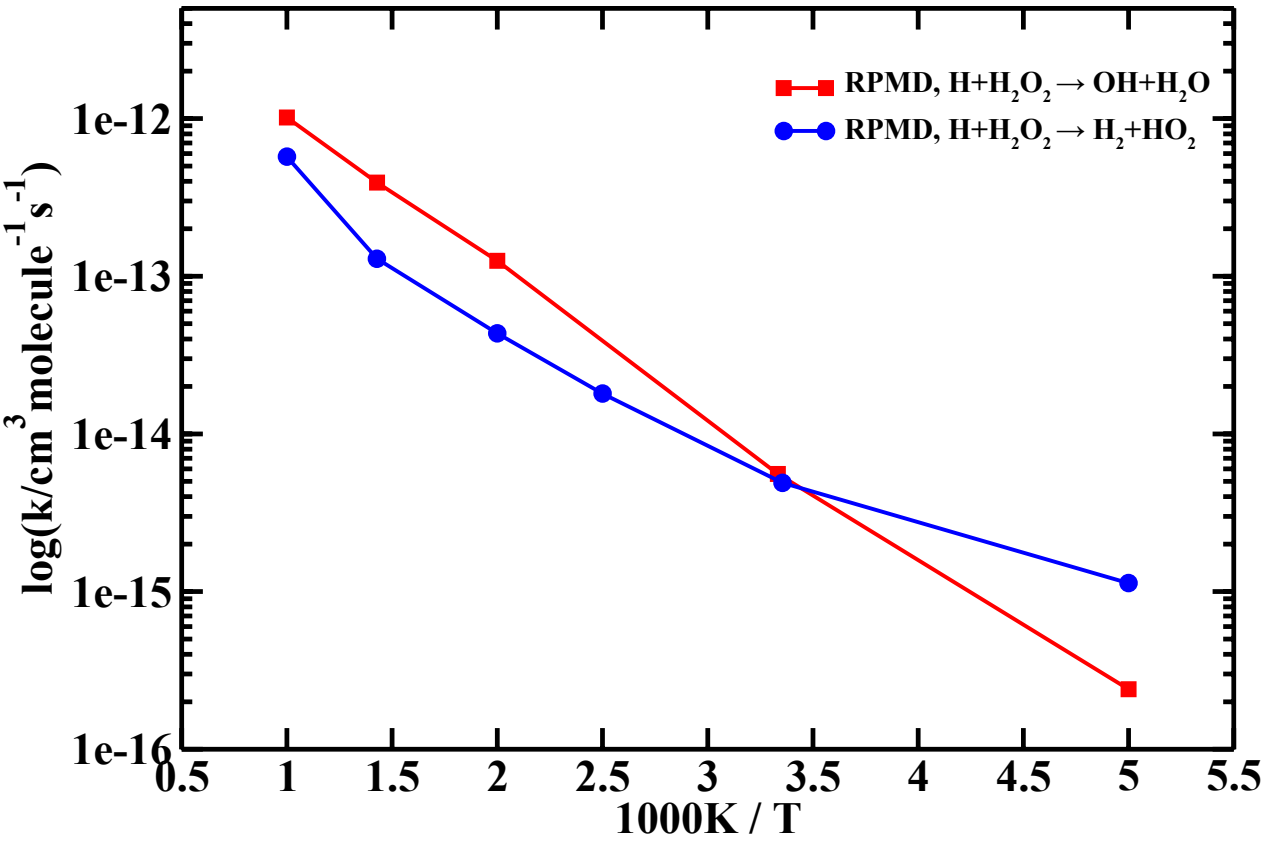
RPMD, H+H2O2 → OH+H2O
RPMD, H+H2O2 → H2+HO2
log(k/cm3molecule-1s-1)
1e-12
1e-13
1e-14
1e-15
1e-16
0.5
1
1.5
2
2.5
3
3.5
4
4.5
5
5.5
1000K / T

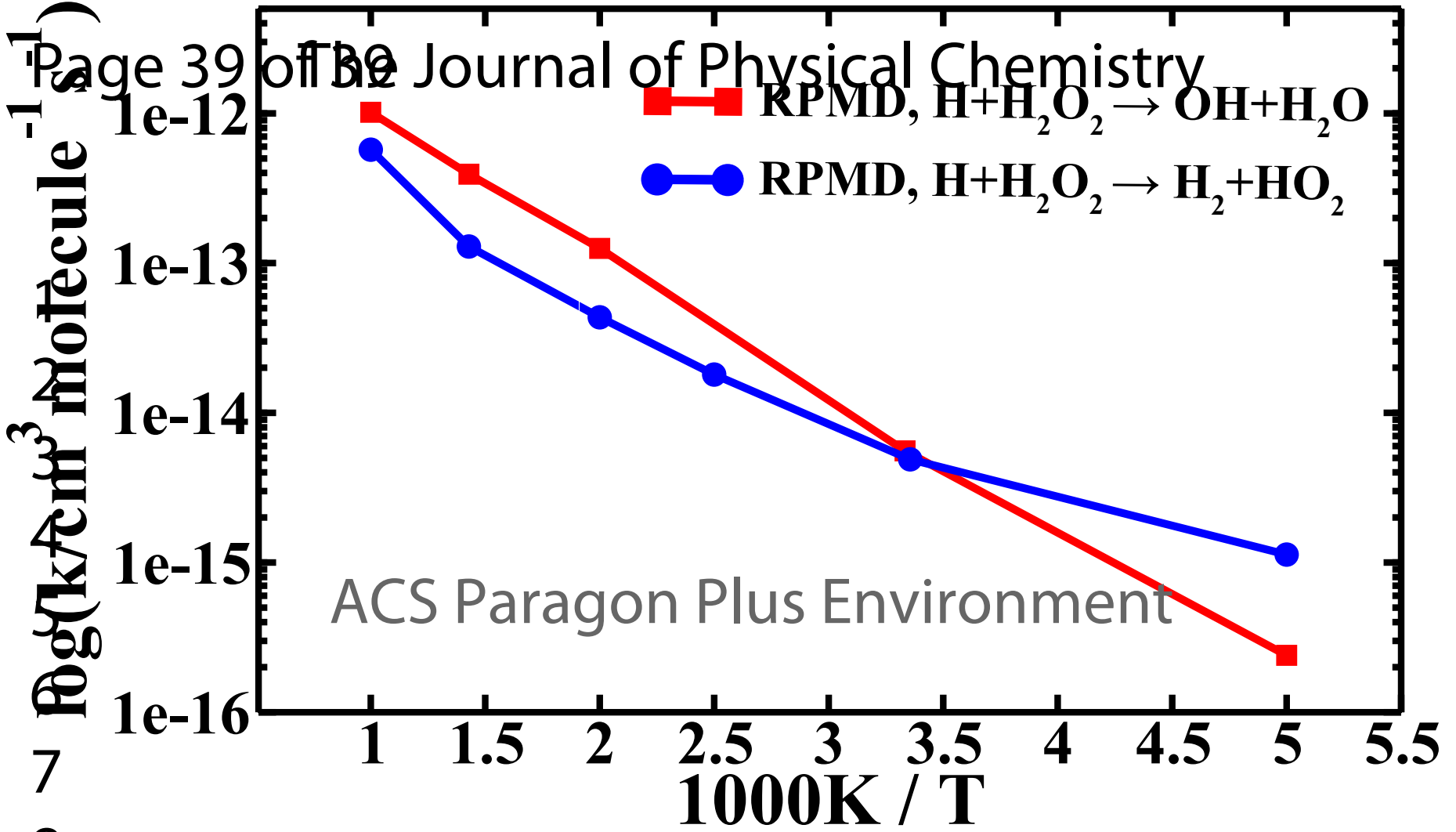
RPMD, H+H2O2 → OH+H2O
RPMD, H+H2O2 → H2+HO2
ACS Paragon Plus Environment
1e-12
1e-13
1e-14
1e-15
1e-16
1
1.5
2
2.5
3
3.5
4
4.5
5
5.5
1000K / T